Application of high-resolution time-of-flight chemical ionization mass spectrometry measurements to estimate volatility distributions of a-pinene and naphthalene oxidation products

Authors: P.S. Chhabra, A.T. Lambe, M.R. Canagaratna, H. Stark, J.T. Jayne, T.B. Onasch, Paul Davidovits, J.R. Kimmel, D.R. Worsnop

Published in *Atmospheric Measurement Techniques*, vol. 8, no. 1, pp. 1-18, 2015

Atmos. Meas. Tech., 8, 1–18, 2015
www.atmos-meas-tech.net/8/1/2015/
doi:10.5194/amt-8-1-2015

Atmospheric Measurement Techniques
Open Access

Application of high-resolution time-of-flight chemical ionization mass spectrometry measurements to estimate volatility distributions of α-pinene and naphthalene oxidation products

P. S. Chhabra[1,*], A. T. Lambe[1,2], M. R. Canagaratna[1], H. Stark[1,3], J. T. Jayne[1], T. B. Onasch[1,2], P. Davidovits[2], J. R. Kimmel[1,3,4], and D. R. Worsnop[1]

[1]Aerodyne Research, Inc. Billerica, Massachusetts, USA
[2]Chemistry Department, Boston College, Chestnut Hill, Massachusetts, USA
[3]Cooperative Institute for Research in Environmental Sciences (CIRES), University of Colorado, Boulder, Colorado, USA
[4]TOFWERK AG, Thun, Switzerland
[*]now at: Department of Chemical Engineering, University of Texas, Austin, Texas, USA

Correspondence to: P. S. Chhabra (pschhabra@utexas.edu)

Received: 19 May 2014 – Published in Atmos. Meas. Tech. Discuss.: 1 July 2014
Revised: 27 October 2014 – Accepted: 24 November 2014 – Published: 5 January 2015

Abstract. Recent developments in high-resolution time-of-flight chemical ionization mass spectrometry (HR-ToF-CIMS) have made it possible to directly detect atmospheric organic compounds in real time with high sensitivity and with little or no fragmentation, including low-volatility, highly oxygenated organic vapors that are precursors to secondary organic aerosol formation. Here, using ions identified by high-resolution spectra from an HR-ToF-CIMS with acetate reagent ion chemistry, we develop an algorithm to estimate the vapor pressures of measured organic acids. The algorithm uses identified ion formulas and calculated double bond equivalencies, information unavailable in quadrupole CIMS technology, as constraints for the number of possible oxygen-containing functional groups. The algorithm is tested with acetate chemical ionization mass spectrometry (acetate-CIMS) spectra of O_3 and OH oxidation products of α-pinene and naphthalene formed in a flow reactor with integrated OH exposures ranged from 1.2×10^{11} to 9.7×10^{11} molec s cm^{-3}, corresponding to approximately 1.0 to 7.5 days of equivalent atmospheric oxidation. Measured gas-phase organic acids are similar to those previously observed in environmental chamber studies. For both precursors, we find that acetate-CIMS spectra capture both functionalization (oxygen addition) and fragmentation (carbon loss) as a function of OH exposure. The level of fragmentation is observed to increase with increased oxidation. The predicted condensed-phase secondary organic aerosol (SOA) average acid yields and O / C and H / C ratios agree within uncertainties with previous chamber and flow reactor measurements and ambient CIMS results. While acetate reagent ion chemistry is used to selectively measure organic acids, in principle this method can be applied to additional reagent ion chemistries depending on the application.

1 Introduction

Oxygenated organics are an abundant class of compounds in the atmosphere, representing significant fractions of the total organic mass in the gas, particle, and cloud droplet phases (Goldstein and Galbally, 2007; Zhang et al., 2007; Jimenez et al., 2009). Much of the oxygenated organic mass is secondary in origin, generated from the gas-phase oxidation (O_3, OH / HO_2 / NO_x, NO_3) of anthropogenic and biogenic volatile organic compounds (VOCs) (Kroll and Seinfeld, 2008; Seinfeld and Pandis, 2006; Goldstein and Galbally, 2007). Recent studies have shown that secondary organic aerosol oxygen content is correlated with the photochemical age of an air mass (Ng et al., 2011; Heald et al., 2010; Jimenez et al., 2009). With increasing oxidation, gas-phase

organic compounds can partition into the particle phase to contribute to secondary organic aerosol (SOA) mass or into the aqueous phase to contribute to water-soluble organic carbon (WSOC) (Hallquist et al., 2009; Ervens et al., 2011; Lim et al., 2010). As a result, their potential impact on climate by increasing and changing the properties of total aerosol mass and cloud condensation nuclei is substantial. However, sources, processing, and sinks of atmospheric organics are poorly characterized owing to their vast chemical complexity (Goldstein and Galbally, 2007). As a result, there is significant uncertainty in modeled secondary organic aerosol loadings and chemistries (Spracklen et al., 2011; Hallquist et al., 2009; Dzepina et al., 2011), necessitating more comprehensive measurements of gas- and particle-phase organics and better predictions of their SOA forming potentials.

Mass spectrometry has become a ubiquitous tool in identifying and quantifying atmospherically relevant organic species. Further, high-resolution mass spectrometry has increasingly become an important technique in elucidating the composition of organics because of its ability to resolve high molecular weight compounds with the same nominal mass with high sensitivity. Offline methods like electrospray ionization coupled with ultrahigh-resolution mass spectrometry are useful in identifying the many different compounds extracted from aerosol filter collection (Laskin et al., 2012; Kundu et al., 2012; Putman et al., 2012) as well as fog samples (Mazzoleni et al., 2010). Such methods, however, are highly selective with variable sensitivities and are not typically suited for online or field measurements. Conversely, the widely used Aerodyne high-resolution time-of-flight aerosol mass spectrometer (HR-ToF-AMS) couples electron ionization with the TOFWERK (Thun, Switzerland) high-resolution time-of-flight mass spectrometer (HTOF) to provide sensitive, quantitative online measurements of organic aerosol elemental composition (Jayne et al., 2000; Canagaratna et al., 2007; DeCarlo et al., 2006; Aiken et al., 2007). The harsh electron ionization of the HR-ToF-AMS limits its speciation capability and introduces uncertainty in its elemental ratio calculation (Chhabra et al., 2011; Farmer et al., 2010; Aiken et al., 2008). Thus, improvements to high-resolution mass spectrometry of atmospherically relevant high molecular weight compounds have sought to combine fast online detection with soft ionization sources (Zahardis et al., 2011).

Recently, the TOFWERK HTOF has been paired with various chemical ionization sources to allow for the sensitive detection of organic compounds at high time resolutions (≤ 1 s) with little to no molecular fragmentation. Chemical ionization sources employ specific reagent ions to initiate reactions that ionize analyte species; different reagent ions tend to be selective to different classes of compounds. The use of acetate chemical ionization mass spectrometry (acetate-CIMS) as a way to quantitatively measure organic acids was first demonstrated by Veres et al. (2008) using a quadrupole mass spectrometer. Veres et al. (2010) used the acetate-CIMS technique to measure acids of carbon number (n_C) 1 to 4, benzenediols, and inorganic acids from biomass burning; furthermore, Veres et al. (2011) used acetate-CIMS to measure small organic acids produced in urban air. Bertram et al. (2011) first described the use of a low-mass resolution ($R = 900$) time-of-flight CIMS which, unlike the quadrupole mass spectrometer, could acquire whole mass spectra at high time resolutions. Yatavelli et al. (2012) demonstrated the potential of a high-mass resolution (HTOF, $R = 4000$) acetate-CIMS to measure a large range ($1 \geq n_C \geq 30$) of organic acids in both particle and gas phases from α-pinene ozonolysis and subsequently used it in a remote forest atmosphere (Yatavelli et al., 2014). Aside from traditional organic acids, the technique has also been used to measure WSOC generated from α-pinene ozonolysis (Aljawhary et al., 2013) and nitrophenols from biomass burning (Mohr et al., 2013). The ability of the HTOF to acquire whole mass spectra at high time and mass resolutions represents a substantial improvement over quadrupole technology.

As soft ionization time-of-flight mass spectrometry techniques become more widely used to study gas- and aerosol-phase organics, methods will be needed to relate the many different species depicted in complex mass spectral data to the physical properties of the detected species. Volatility, expressed as vapor pressure, p^0, or saturated mass concentration, c^*, is an important property that governs whether a species partitions into the condensed phase. There has been much effort to relate HR-ToF-AMS data to volatility; thermal denuder measurements and dilution experiments with the AMS have been used to constrain the volatility of organic aerosol (Cappa and Jimenez, 2010; Cappa, 2010; Huffman et al., 2009). The lack of carbon number information from AMS data, a key input in volatility prediction models, may produce uncertainty. Soft ionization high-resolution mass spectrometry retains full molecular information in its spectra, i.e., the chemical formula, $C_xH_yO_z$, of unfragmented parent molecules can be obtained. Thus, it has the potential to provide the inputs for more accurate volatility estimations.

In this study, we explore the high-resolution acetate-CIMS spectra of photochemically produced organic acids and predict the volatility of the species detected. Acids are of particular interest because carboxylic acid functionality dramatically reduces the vapor pressure of its parent molecule and also represents the oxidative endpoint for a terminal carbon before fragmentation. Carboxylic acids also contribute a significant portion of total SOA mass (Ng et al., 2011; Vogel et al., 2013). We choose to examine the α-pinene, and naphthalene systems because their gas-phase compositions and mechanisms have been studied in detail, and various acids have been identified in each system (Yu et al., 1999; Claeys et al., 2013; Kautzman et al., 2009). Using the Van Krevelen diagram (hydrogen-to-carbon ratio, H / C, plotted against the oxygen-to-carbon ratio, O / C) and Kroll diagram (oxidation state, OS_C, plotted against carbon number, n_C), we identify small organic acids and tracer compounds and examine

the changing distributions of carbon as a function of OH-exposure for the first time using the potential aerosol mass (PAM) flow reactor. We note that the high-resolution time-of-flight chemical ionization mass spectrometry (HR-ToF-CIMS) spectra contain many different mass-to-charge ions – on the order of 100 or more unknown ions. Since calibration of each individual measured species may not be feasible due to unknown identity or unavailability of standards, we adopt a simplifying approach in which the measured species are quantified using an average calibration value for organic acids. Acetate ionization may have an advantage in this respect since it is primarily selective for acids. While this assumption can lead to larger errors for any given individual species, it allows for a practical way of calculating average (ensemble) properties and mass concentrations for the large number of organic ions in the HR-ToF-CIMS spectra. This will be an on going developmental issue with the HR-ToF-CIMS systems and the uncertainty it introduces will be discussed. Additionally, we develop an algorithm to estimate the volatility of the species detected in each system and discuss the implications of the results.

2 Experimental method and data analysis

2.1 Acetate-CIMS

The Aerodyne HR-ToF-CIMS, hereby referred to as the CIMS, using acetate reagent ion chemistry has been described in detail in previous publications (Bertram et al., 2011; Yatavelli et al., 2012). A sample from the PAM reactor is drawn through a critical orifice at $2.0\,\mathrm{L\,min^{-1}}$ into the ion-molecular reaction (IMR) chamber. Acetate reagent ions are generated by bubbling approximately 200 sccm of N_2 through a reservoir of acetic anhydride, diluting the flow to $2\,\mathrm{L\,min^{-1}}$ with N_2 and passing it through a commercial ^{210}Po alpha emitter (P-2021, NRD) before introducing it into the IMR orthogonally to the sample flow (Veres et al., 2008). Within the IMR, acetate ions abstract protons from acids having gas-phase acidities greater than that of acetic acid or cluster with gas-phase species to form adduct ions, as shown in Reactions (R1) and (R2).

$$CH_3CO(O)O^- + HX \rightarrow CH_3C(O)OH + X^- \quad \text{(R1)}$$

$$CH_3CO(O)O^- + HX \rightarrow CH_3C(O)O^-(HX) \quad \text{(R2)}$$

The IMR (100 mbar) is coupled to the HTOF mass analyzer (1×10^{-7} mbar) by a series of differentially pumped stages that includes DC and RF focusing optics (AP interface). The first pumping stage contains a segmented, RF-only quadrupole operated at 2 mbar. Voltages in this quadrupole can be tuned to transmit (weak field) or dissociate (strong field) non-covalent clusters. In these experiments, voltages were adjusted in order to minimize the clustering, as indicated by the by the signal at m/z 119 (acetic acid acetate cluster, $C_4H_7O_4^-$). As a result, during normal operation, the ratio between m/z 59 (acetate reagent ion, $C_2H_3O_2^-$) and m/z 119 was approximately 5 to 1.

The ion source is coupled to a TOFWERK HTOF, identical to the mass spectrometer of the Aerodyne HR-ToF-AMS (DeCarlo et al., 2006; Canagaratna et al., 2007). The HTOF is capable of running in both positive and negative polarities but only the negative polarity was operated due to the reagent ion scheme. As with the Aerodyne HR-ToF-AMS (henceforth referred to as the AMS), the CIMS can be operated in a higher sensitivity, lower-resolution V-mode, or a lower sensitivity, higher-resolution W-mode. All experiments presented here were performed in V-mode. Although the HTOF is identical, the effective resolution of the CIMS is better than the AMS since the ion source is cooler in the former. In these experiments, the achieved resolution was approximately 4000.

A formic acid sensitivity calibration of the acetate-CIMS was conducted by flowing N_2 over a constant temperature permeation tube which itself was calibrated using an Aerodyne Quantum Cascade Laser Tracer Gas Monitor (Herndon et al., 2007). We determined a sensitivity of $5.5\pm0.9\,\mathrm{Hz\,ppt^{-1}}$ at an extraction frequency of 16.7 kHz, similar to the sensitivity $3\,\mathrm{Hz\,ppt^{-1}}$ at an extraction frequency of 25 kHz found by Yatavelli et al. (2012). Based on previous acetate-CIMS studies (listed in Table S1 in the Supplement), we assume a constant relative ionization efficiency of 1.3 ± 0.8 for all other species.

2.2 Organic vapor and aerosol production

Figure 1 shows a schematic of the experimental setup. Oxidized organic vapors were generated in a PAM flow reactor (Kang et al., 2007; Lambe et al., 2011a). The PAM reactor is a horizontal 13.3 L glass cylindrical chamber through which a carrier gas of N_2 and O_2 flowed at rates of 8.5 and $0.5\,\mathrm{L\,min^{-1}}$, respectively. Four mercury lamps (BHK Inc.) with peak emission intensity at $\lambda = 254$ nm are mounted in teflon-coated quartz sleeves inside the chamber and are flushed continuously with N_2. The CIMS was connected to the outlet of the PAM reactor with 0.635 cm (1/4 in.) OD, 0.476 cm (3/16 in.) ID PFA tubing, approximately 0.46 m (1.5 ft) long and was heated to 200 °C. These conditions were chosen to maintain laminar flow and to minimize condensation of organic vapors within the tube. Thus, collected spectra represent the combined contribution of gas-phase and particle-phase organics

OH radicals were produced via the reaction $O_3 + h\nu \rightarrow O_2 + O(^1D)$ followed by the reaction $O(^1D) + H_2O \rightarrow 2OH$. O_3 was generated by irradiating O_2 in the carrier gas flow with a mercury Pen-Ray™ lamp ($\lambda = 185$ nm) before it entered the PAM reactor. Ozone concentrations were measured using an O_3 monitor (2B Technologies); O_3 ranged between 5 ppm at the highest OH exposures to 6 ppm for ozonolysis experiments. Water vapor (~ 30 %) was introduced by humidifying the carrier N_2 flow using a Nafion™ membrane humidifier. OH exposure was varied by changing the volt-

Table 1. Experimental conditions and results.

Expt no.	VOC system	VOC conc. (ppb)	OH exposure (molec s cm^{-3})	OH days[a]	$\overline{n_C}$[b]	$\overline{O/C}$[c]	$\overline{H/C}$[d]	$\overline{OS_C}$[e]
1	α-pinene + O_3	15	–	–	3.35	0.84	1.46	0.23
2	α-pinene + O_3	30	–	–	4.08	0.73	1.47	−0.02
3	α-pinene + OH	15	3.7×10^{11}	2.8	3.41	0.90	1.39	0.41
4	α-pinene + OH	15	7.0×10^{11}	5.4	2.97	1.02	1.34	0.71
5	α-pinene + OH	30	7.0×10^{11}	5.4	3.17	0.99	1.33	0.65
6	α-pinene + OH	30	9.7×10^{11}	7.5	3.09	1.01	1.32	0.71
7	α-pinene + OH	15	9.7×10^{11}	7.5	3.03	1.01	1.32	0.70
8	naphthalene + OH	23[f]	1.2×10^{11}	0.96	3.55	0.99	1.29	0.69
9	naphthalene + OH	46[f]	1.2×10^{11}	0.96	4.92	0.75	1.18	0.32
10	naphthalene + OH	46[f]	1.2×10^{11}	0.96	4.56	0.84	1.28	0.40
11	naphthalene + OH	23[f]	1.9×10^{11}	1.5	4.42	0.85	1.29	0.41
12	naphthalene + OH	23[f]	2.8×10^{11}	2.1	4.51	0.79	1.16	0.42
13	naphthalene + OH	23[f]	3.7×10^{11}	2.8	3.40	0.94	1.16	0.72
14	naphthalene + OH	23[f]	5.3×10^{11}	4.1	2.85	1.08	1.21	0.94
15	naphthalene + OH	23[f]	9.7×10^{11}	7.5	2.80	1.08	1.22	0.94

[a] Based on a diurnally averaged OH concentration of 1.5×10^6 molec cm^{-3}. [b] Average carbon number. [c] Average oxygen-to-carbon ratio. [d] Average hydrogen-to-carbon ratio. [e] Average carbon oxidation state. [f] Concentration estimated from equilibrium vapor pressure at 25 °C.

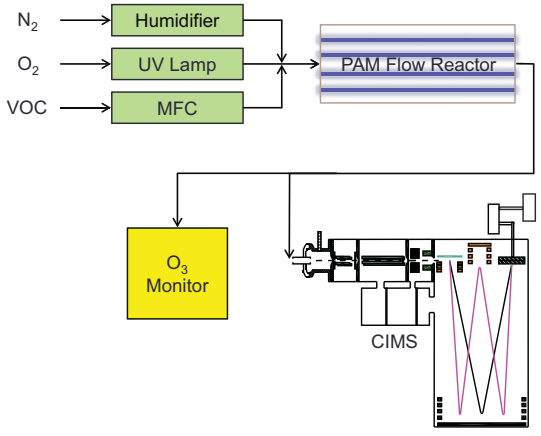

Figure 1. Schematic of the experimental setup. CIMS diagram adapted from Fig. 2 of Yatavelli et al. (2012).

age applied to the PAM reactor lamps between 0 and 110 V. The OH exposure was calculated by measuring the decay of (^{2}H)formic acid (measured in high-resolution spectra at $m/z = 46.00393$, as deuterated formate ion $DCOO^-$) introduced into the PAM reactor with a permeation tube assuming $k_{OH} = 4.62 \times 10^{-13}$ cm^3 molec^{-1} s^{-1} (Wine et al., 1985).

Although ozone concentrations were similar between ozonolysis and photooxidation experiments, OH concentrations were high enough that α-pinene + OH ($k_{OH} = 5.4 \times 10^{-11}$ cm^3 molecule^{-1} s^{-1}) reactions are 5 to 40 times faster than ozonolysis reactions ($k_{O_3} = 8.7 \times 10^{-17}$ cm^3 molecule^{-1}s^{-1}), and naphthalene + OH ($k_{OH} = 2.59 \times 10^{-11}$ cm^3 molecule^{-1} s^{-1}) reactions are 700 to 5700 times faster than ozonolysis ($k_{O_3} = 3 \times 10^{-19}$ cm^3 molecule^{-1} s^{-1}) reactions (Atkinson and Aschmann, 1986; Seinfeld and Pandis, 2006). These calculations suggest that photooxidation products measured with the CIMS are mostly from OH reactions, although we cannot completely rule out minor contributions from O_3 reactions particularly at the lowest OH exposures that were used.

Typical OH exposures ranged from 1.2×10^{11} to 9.7×10^{11} molec s cm^{-3} which is equivalent to 1.0–7.5 days of atmospheric oxidation assuming an average atmospheric OH concentration of 1.5×10^6 molec cm^{-3} (Mao et al., 2009). Ozonolysis experiments were performed by turning the UV lamps off. OH exposures in units of molec s cm^{-3} and equivalent atmospheric exposure times in OH Days are listed in Table 1. Before each experiment, the PAM flow reactor was conditioned with OH radicals until a particle background of less than 10 particles cm^{-3} was achieved.

The VOC precursors investigated in this study were α-pinene and naphthalene. α-pinene was prepared in compressed gas cylinders at known concentrations and introduced into the PAM reactor at controlled rates using a mass-flow controller. Naphthalene vapor was introduced by flowing N_2 over solid naphthalene placed in a Teflon tube (Chan et al., 2009). Naphthalene concentrations listed in Table 1 are estimated from equilibrium vapor pressures at 25 °C. We estimate an error of 38 % in the naphthalene concentrations based on the variability of literature vapor pressure values. Additionally, we estimate a 20 % error in the α-pinene concentrations. The VOC concentrations that were used resulted in particle mass loadings ≤ 7 µg m^{-3} (assuming SOA density of 1.4 g cm^{-3}), measured after the heated sample

line, or approximately 3 % of the total organic carbon. Thus, the influence of slowly evaporating organic aerosols in the heated sample line after the PAM chamber on total gas-phase CIMS measurements is likely minimal under these conditions. Additional uncertainties in the measurements due to PAM-specific issues, such as direct photochemistry, wall effects, and high OH concentrations, have been discussed in detail in Lambe et al. (2011a, 2012).

2.3 Data analysis

Spectral data were analyzed using the Tofware (TOFWERK and Aerodyne) toolkit, developed for the IGOR Pro 6.x analysis software (WaveMetrics, Lake Oswego, OR, USA). Similar to the Squirrel and PIKA toolkits developed for Aerodyne AMS data, the Tofware software can index, preprocess (m/z calibration, baseline correction, and peak interpretation), and integrate raw mass spectra to produce unit mass resolution (UMR) data or take advantage of the high-resolution capability of the HTOF to assign signal contributions to individual ions with different elemental compositions. The latter method allows for the calculation of bulk elemental ratios ($\overline{\mathrm{O/C}}$, $\overline{\mathrm{H/C}}$), carbon numbers ($\overline{n_C}$), and carbon oxidation states ($\overline{\mathrm{OS_c}}$) (Kroll et al., 2009). Here, we calculated O / C, H / C, $\mathrm{OS_c}$, and n_C values assuming all measured ions are (1) produced from reactions with the acetate reagent ion (Reactions R1 and R2) and (2) have the same ionization efficiency.

All HR mass spectra were blank corrected using measurements of the PAM reactor outflow in the absence of VOC precursors. Spectra were normalized to the acetate reagent ion signal at m/z 59 to account for variations in the source and analyte loadings. We assumed that all identified peaks were molecular anions formed from Reaction (R1) ($\mathrm{M^-}$) or cluster ions formed from Reaction (R2) ($\mathrm{CH_3C(O)O^-(MH)}$); the latter were corrected using the method described below. Since no chemically labile nitrogen was added to the experiments, it was assumed no nitrogen-containing molecules were generated in the PAM. Thus, ions with even nominal masses were not included in the fitted peak list except for even-mass isotopes of odd-mass parent ions, constrained by their natural abundances. Signals at nominally even mass to charges were dominated by $\mathrm{NO_2^-}$ and $\mathrm{NO_3^-}$, originating as contaminate signal from metal tubing and the ionizer. By summing high-resolution signals from even-massed ions that are not inorganic or isotopes of odd-massed ions, we estimate that less than 7 % of the signal at even masses is from organic ions. Using these criteria, approximately 350 molecular ions were fitted in each system. Of the total number of fitted ions, only those which had a blank subtracted signal greater than 1 standard deviation (1σ) of the time-averaged signal were included in the analysis, approximately 100–200 ions.

Adduct ion signals in the CIMS spectra have the potential to bias the measured composition toward higher molecular weight species. However, because of the elemental composition of acetate, distinguishing adduct ion signal from true molecular ion signal is not straightforward. To estimate adduct ion contributions, we first define that a non-clustered base ion has a molecular formula i, and when the acetate mass is added, its formula is $i + \mathrm{C_2H_4O_2}$. We denote the adduct ion as i' and a non-clustered ion at the same mass as j. The signal at the clustered mass, $I_{i+\mathrm{C_2H_4O_2}}$ is equal to the sum of the adduct ion signal $I_{i'}$ and non-adduct ion signal I_j:

$$I_{i+\mathrm{C_2H_4O_2}} = I_{i'} + I_j. \quad (1)$$

We assume that across all experiments of a given precursor, the ratio of $I_{i'}$ to I_i is constant and is no more than the ratio of signal at m/z 119 to signal at m/z 59, or 0.2. The ratio of $I_{i+\mathrm{C_2H_4O_2}}$ to I_i represents an upper bound to this value. Thus, across all experiments of a given precursor, the minimum ratio of $I_{i+\mathrm{C_2H_4O_2}}$ to I_i or 0.20, whichever is smaller, is used to approximate the ratio of $I_{i'}$ to I_i. In other words,

$$I_{i'} \approx \min\left\{\frac{I_{i+\mathrm{C_2H_4O_2}}}{I_i}, 0.2\right\} \times I_i. \quad (2)$$

To correct for clustering, the estimated value of $I_{i'}$ calculated from Eq. (2) is added back to I_i and subtracted from $I_{i+\mathrm{C_2H_4O_2}}$. The effect of this correction on bulk composition values is minimal, on the order of a couple percent. The true clustering correction (and associated uncertainty) is likely significantly larger for individual molecules due to compound-specific acetate proton transfer reaction rates that are not known. Figures S3 and S4 in the Supplement illustrate how much signal in example spectra is estimated to be from clustering and redistributed to base ion signals.

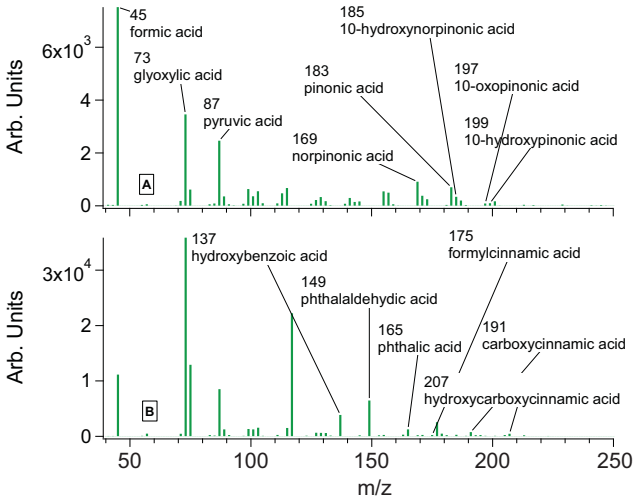

Figure 2. Acetate-CIMS unit mass resolution spectra of α-pinene ozonolysis (**a**, Expt 1), and naphthalene photooxidation (**b**, Expt 12). Even-massed ions, reagent ions, and dominant background ions are removed, and blank spectra are subtracted. Select ions identified in previous studies are labeled (Yu et al., 1999; Kautzman et al., 2009).

CIMS spectra of oxidized organic vapors produced from naphthalene contained contaminant ion signals from the α-pinene products. To remove ions overlapping both systems, an α-pinene spectra corresponding to the nearest exposure and normalized to the $C_9H_{14}O_3^-$ ion was subtracted from the naphthalene spectra (possibly introducing some additional uncertainty in small acid signals). Subsequently, because of the highly unsaturated nature of naphthalene tracer products (H / C < 1) some ions could be exclusively attributed to α-pinene ($n_C \geq 6$ and H / C > 1, supported by the spectral separation in Van Krevelen space illustrated in Fig. 3) and were removed.

2.4 Volatility estimation method

In this work, we use SIMPOL.1 (Pankow and Asher, 2008) to predict the vapor pressures of the species detected by the acetate-CIMS. The challenge in applying SIMPOL to conventional electron ionization mass spectra, e.g., AMS, is that the average carbon number ($\overline{n_C}$) and functional group composition needed as inputs are both typically unknown. This makes it necessary to calculate $\overline{n_C}$ indirectly, which introduces additional uncertainty (Daumit et al., 2013; Donahue et al., 2011; Kessler et al., 2010, 2012). Simplifying assumptions must also be made about the functional group composition and their effect on vapor pressure (Donahue et al., 2011; Cappa and Wilson, 2012). However, soft ionization techniques, such as acetate-CIMS, generate mass spectra that retain the unfragmented parent ions; thus, molecular formulas are known. This makes determination of the functional group composition more straightforward.

Here, we expand upon the work of Daumit et al. (2013) to determine functional group composition with additional constraints provided by high-resolution acetate-CIMS. Because acetate ionization is sensitive to acids, we assume at least one carboxylic acid functionality is present provided there are at least two oxygens in the molecule and at least one site of unsaturation. The number of sites of unsaturation is determined by the double bond equivalency (DBE, i.e., degrees of unsaturation) formula:

$$\mathrm{DBE} = 1 + n_C - \frac{1}{2} n_H. \quad (3)$$

The remaining sites of unsaturation are referred to as $\mathrm{DBE_r}$ (which is one less than DBE if there is an acid group present). We assume that the remaining oxygen, n_{rO} (which is two less than the total if there is an acid group present), are either contained in hydroxyl (-OH) or keto (=O) groups and that any extra acid groups are a combination of one of each:

$$n_{rO} = n_{\text{-OH}} + n_{=O}. \quad (4)$$

We assume that other oxygen-containing functional groups that may be present in the spectra are well represented by ketone and/or hydroxyl surrogates. This assumption is reasonable for epoxide groups that have similar bonding as carbonyls, but not for other functional groups such as acyclic

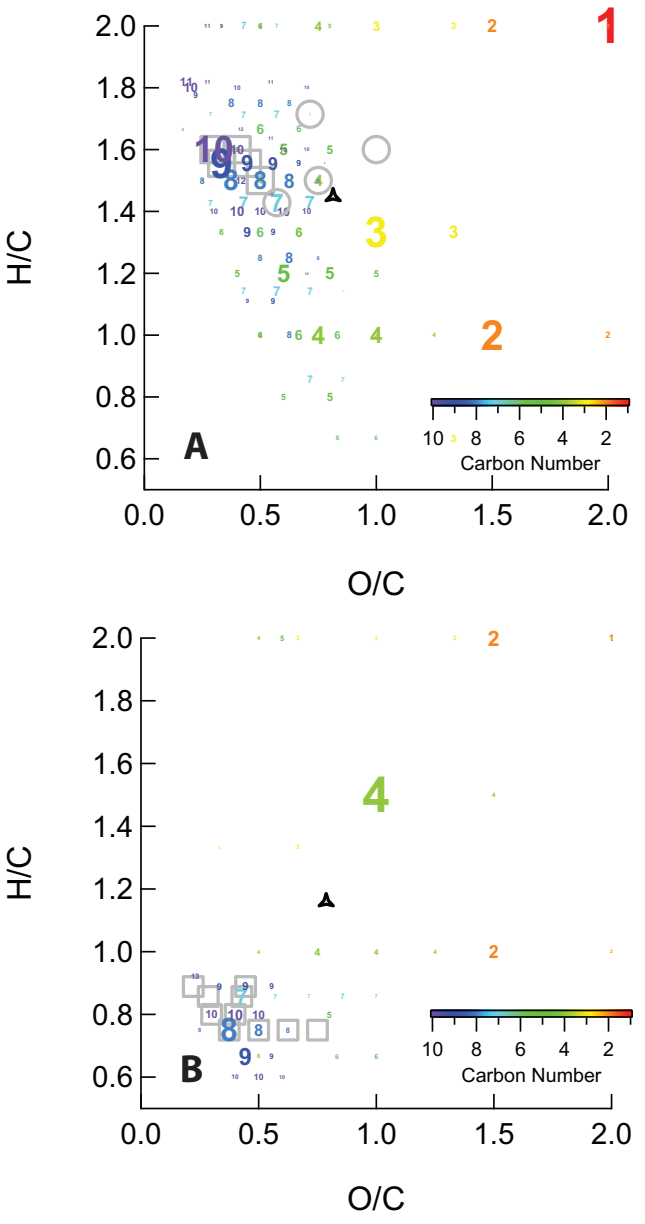

Figure 3. Modified Van Krevelen diagram of gas-phase acetate-CIMS high-resolution spectra of **(a)** α-pinene ozonolysis (Expt 1) and **(b)** naphthalene photooxidation (Expt 12). Each integer marker represents a fitted ion with the number representing the carbon number of the ion. The color bar is representative of the carbon number range of the high-resolution spectrum. The size of each number is proportional to the carbon number-weighted signal of its corresponding ion; the largest markers in **(a)** and **(b)** represent 11 % and 38 % of the carbon-weighted signal, respectively. Gray square markers in **(a)** indicate tracer acids identified by Yu et al. (1999) and gray circle markers indicate SOA tracer acids noted in Claeys et al. (2013). Gray square markers in **(b)** indicate tracer acids identified by Kautzman et al. (2009). Names and locations of acids on the VK are shown in the Supplement, Figs. S5 and S6. The bulk O / C and H / C values are marked by black triangles.

ethers, esters, or hydroperoxides that might be present (Daumit et al., 2013).

If $n_{rO} \leq DBE_r$ then all oxygens are assigned as carbonyls and the remaining sites of unsaturation are considered C = C double bonds:

$$n_{rO} = n_{=O}, \quad (5)$$

$$n_{\text{-OH}} = 0, \quad (6)$$

$$DBE_r - n_{=O} = n_{C=C}. \quad (7)$$

If $n_{rO} > DBE_r$ then all remaining sites of unsaturation are considered to be carbonyl groups and the remainder oxygens are hydroxyl groups:

$$n_{=O} = DBE_r, \quad (8)$$

$$n_{\text{-OH}} = n_{rO} - n_{=O}. \quad (9)$$

Pairs of carbonyls and hydroxyl groups are combined to form additional carboxylic acid groups, with the total number of acid groups constrained to no more than two assuming linear carbon chains.

Additional constraints can be applied as needed if more information is known. For example α-pinene oxidation products often retain a four-carbon ring; thus, we impose the constraint that if $n_C > 8$ and $DBE_r \geq 1$, a non-aromatic ring functionality (n_r) is added to the SIMPOL calculation. Likewise, for naphthalene spectra, if $n_C > 6$ and $DBE_r \geq 4$, then at most one aromatic ring functionality is added (n_{Ar}, equivalent to four sites of unsaturation). In both cases these steps are done after the initial acid is assigned and the DBE_r is updated.

Algorithm outputs from Eqs. (3) to (9) are used as inputs to the SIMPOL model, which parameterizes the vapor pressure of a pure compound as a linear combination of contributions from its functional groups:

$$\log_{10}\left(p^0_{L,i}\right) = b(T)_0 + \sum_k n_{k,i} b(T)_k, \quad (10)$$

where $b(T)_k$ is the temperature-dependent contribution term of functional group k and $n_{k,i}$ is the number of functional groups of type k in species i; $b(T)_0$ is a constant term. For example, the addition of a hydroxyl group lowers the vapor pressure by a factor of $10^{2.23}$ at 293 K; this is represented as $b(293\,\text{K})_{OH} = -2.23$. To convert p^0 to c^*, an additional term is added to the above equation:

$$\log_{10}\left(c^*_i\right) = \log_{10}\alpha + b(T)_0 + \sum_k n_{k,i} b(T)_k, \quad (11)$$

where $\alpha = \frac{10^6 \times MW_i}{RT}$ which equals 8.314×10^9 at 293 K. The factor MW_i refers to the molecular weight of species i, R is the ideal gas constant (8.21×10^{-5} atm m^3 mol^{-1} K^{-1}), and T is the temperature (293 K). Technically, c^* is the product of the saturation concentration of the pure sub-cooled liquid, c^0, and its activity coefficient in solution γ, but the activity coefficient is assumed to be unity. Derivation of the estimation in uncertainty in SIMPOL vapor pressure prediction is detailed in the Supplement.

Table 2 lists several example oxidation products from each experimental system along with the number of each functional group assigned to it. Across the top of the table are the values of each group contribution term used in this work. The calculated c^* for product is listed at the right of the table.

3 Results

3.1 CIMS Spectra, $\overline{O/C}$ and $\overline{H/C}$ ratios, $\overline{n_C}$

Figure 2 displays representative UMR spectra obtained from α-pinene ozonolysis and naphthalene photooxidation conditions in the PAM reactor. In all cases the largest signals are observed at m/z 45, 73, 75, and 87, which correspond to formic acid, glyoxylic acid, glycolic acid, and pyruvic acid, respectively. The prominence of these small acids in acetate-CIMS spectra has been previously observed by Yatavelli et al. (2012). Production of small acids in urban atmospheres has been correlated with photochemical activity (Veres et al., 2011) and although their exact formation mechanism is unknown, it is likely they are generated from the oxidative fragmentation of the parent VOCs and subsequent products.

Analyzing the mass spectra shown in Fig. 2 in high resolution allows for calculation of average oxygen-to-carbon and hydrogen-to-carbon ratios ($\overline{O/C}$ and $\overline{H/C}$), average carbon oxidation states ($\overline{OS_C}$), and average carbon numbers ($\overline{n_C}$). Table 1 presents $\overline{O/C}$, $\overline{H/C}$, $\overline{OS_C}$, and $\overline{n_C}$ for all of the studied conditions. In general, these parameters follow the expected trends as a function of precursor type and OH exposure. First the $\overline{n_C}$ values of α-pinene ($\overline{n_C} = 2.97$–4.08) and naphthalene ($\overline{n_C} = 2.80$–4.92) oxidation products span similar ranges with the $\overline{OS_C}$ values of naphthalene being generally higher than those of α-pinene, especially at low OH exposures. This is consistent with naphthalene itself having a higher $\overline{OS_C}$ value than α-pinene. Second, the average $\overline{OS_C}$ and $\overline{O/C}$ for α-pinene and naphthalene oxidation products increase with increasing OH exposure while the average $\overline{n_C}$ decreases with OH exposure. Third, α-pinene oxidation products have higher $\overline{H/C}$ ratios than naphthalene, consistent with previous studies (Chhabra et al., 2011; Lambe et al., 2011b).

3.2 Van Krevelen diagram

A Van Krevelen diagram can be used to plot the corresponding H / C and O / C ratios of ions presented in the mass spectra. Figure 3a shows a Van Krevelen diagram corresponding to the α-pinene ozonolysis spectrum presented in Fig. 2a. Markers are numbered and colored by n_C, sized by the ion signal intensity, and weighted by n_C to emphasize the distribution of carbon across the spectra. Identified ions with known chemical formulae are marked with gray cir-

Table 2. Examples of detected species, their double bond equivalencies (DBE $= 1+n_C-\frac{1}{2}n_H$), and their calculated saturation concentrations based on the number of each type of functional group, n_k. Note that DBE $= n_{=O}+n_{C(O)OH}+n_{C=C}+n_r+4\times n_{Ar}$. Values in parentheses are the SIMPOL group contribution coefficients for the corresponding functional group (Pankow and Asher, 2008). Underneath each type of functional group, the associated additivity constant is shown. Errors are calculated based on the method detailed in the Supplement.

Species Formula	DBE	Constant ($b_0 = 1.79$)	n_C ($b_1 = -0.44$)	$n_{=O}$ ($b_9 = -0.94$)	n_{-OH} ($b_7 = -2.23$)	$n_{C(O)OH}$ ($b_{10} - 3.58$)	$n_{C=C}$ ($b_5 = -0.10$)	n_r ($b_4 = -0.01$)	n_{Ar} ($b_3 = -0.68$)	$\log c^*$	c^* ($\mu g\,m^{-3}$)
α-pinene											
$C_9H_{14}O_4$	3		9			2		1		0.60 ± 1.0	3.68 ± 8.47
$C_{10}H_{14}O_7$	4		10	1	2	2		1		-5.14 ± 3.38	$7.15\times10^{-6} \pm 5.56\times10^{-5}$
$C_8H_{12}O_6$	3		8	1	1	2				-2.12 ± 1.70	$7.53\times10^{-3} \pm 3.04\times10^{-2}$
naphthalene											
$C_8H_6O_3$	6		8	1		1			1	2.89 ± 0.61	$7.77\times10^{2} \pm 1.08\times10^{3}$
$C_9H_6O_4$	7		9	2		1			1	1.59 ± 0.74	$4.28\times10^{1} \pm 67$

cles and squares in Fig. 3a (squares: Yu et al., 1999; circles: Claeys et al., 2013; proposed identities are given in Fig. S5 in the Supplement). Figure 3a illustrates those ions with $n_C = 1$ to 12 are measured by the acetate-CIMS for α-pinene ozonolysis. Much of the carbon ($\sim 45\,\%$) is characterized by molecules with O / C = 0.3 to 0.7 and $n_C = 7$ to 10, including ions corresponding to well-characterized gas-phase oxidation products, such as $C_{10}H_{16}O_3$ (pinic acid) and norpinonic acid ($C_{10}H_{14}O_3$), which by themselves contribute $\sim 14\,\%$ of the measured carbon. Other $n_C = 10$ ions are also detected, with O / C values as high as 0.7 such as $C_{10}H_{16}O_7$ and $C_{10}H_{14}O_7$. Highly oxidized ions with these formulas have been previously measured by Ehn et al. (2012) in ambient and chamber experiments. The acids identified by Yu et al. (1999) contribute approximately 20 % to the measured carbon of acidic α-pinene ozonolysis products. Acids identified by Claeys et al. (2013), such as 3-methyl-1,2,3-butanetricarboxylic acid (MBTCA, $C_8H_{12}O_6$) and terebic acid ($C_7H_{10}O_4$), have smaller contributions on the order of $\sim 3\,\%$.

Approximately 33 % of the carbon is contained in small highly oxidized acids with $n_C = 1$ to 3 and O / C ≥ 1. Because the relative abundance of these acids increases as a function of OH exposure they are presumably formed following fragmentation of early generation oxidation products with larger n_C. Small-n_C ions with large signals include CH_2O_2 (formic acid), $C_2H_2O_3$ (glyoxylic acid), and $C_3H_4O_3$ (pyruvic acid) which represent 26 % of the total carbon measured for α-pinene ozonolysis products.

The formation of formic acid from α-pinene ozonolysis and photooxidation has been previously observed in several studies (Lee et al., 2006a, b; Librando and Tringali, 2005; Orlando et al., 2000). We measured a formic acid molar yield from α-pinene ozonolysis of 10 %, which is similar to the molar yield of 7.5 % previously observed by Lee et al. (2006a). Given that our experiments were performed under low-NO_x conditions, it is possible that formic acid was formed via the reaction of formaldehyde with HO_2 (Su et al., 1979). Orlando et al. (2000) also proposed formic acid as a first generation product from terpene-OH reactions. Formation of glyoxylic acid and glycolic acid from the gas-phase oxidation of α-pinene or naphthalene has not previously been reported. We note that glyoxal can be produced from the photooxidation of terpenes (Fu et al., 2008) and naphthalene (Nishino et al., 2009), and that glyoxal may be a source of glyoxylic and glycolic acid (Galloway et al., 2009; Lim et al., 2010). Similarly, methylglyoxal is also a product of terpene oxidation (Fu et al., 2008) and is a possible source of pyruvic acid (Lim et al., 2010).

The Van Krevelen diagram of naphthalene is shown in Fig. 3b. Measured naphthalene oxidation products that have been observed in previous chamber studies (depicted by gray square boxes, proposed identities given in Fig. S6 in the Supplement) represent at most 33 % of the carbon and include $C_8H_6O_3$ (phthalaldehydic acid), $C_8H_6O_4$ (phthalic acid), and $C_{10}H_8O_3$ (formylcinnamic acid) (Kautzman et al., 2009). We measured several oxidation products with $n_C = 9$ and 10, including $C_9H_6O_4$ and $C_{10}H_8O_5$ that to our knowledge have not been previously identified. In naphthalene spectra, a strong $C_4H_5O_4$ ion signal was detected that corresponds to a previously unidentified compound. Two possible structures are (1) a diacid with two saturated, unoxygenated carbons, or (2) a mono-acid with one double bond and two hydroxyl groups, which may be more plausible.

3.3 Oxidation state vs. carbon number

Figure 4 displays oxidation state as a function of carbon number for α-pinene and naphthalene oxidation products as a function of OH exposure. The utility of plotting OS_C as a function of n_C (i.e., Kroll Diagram) was introduced by Kroll et al. (2011) to provide a visualization of the chemical complexity of atmospheric organics and their corresponding oxidation trajectories. The top inset panels show the fraction of carbon signal as a function of n_C. A multimodal n_C distribution is observed for α-pinene and naphthalene oxidation products (Fig. 4a and b top insets). The mode defined by $n_C = 8$ to 10 species can be viewed as functionalized products where a net addition of oxygen occurs while the carbon backbone of the precursor is mostly retained (Lambe et al., 2012; Kroll et al., 2009). Figure 4a and b show that the fraction of acids with $n_C = 8$ to 10 decrease as a function of OH

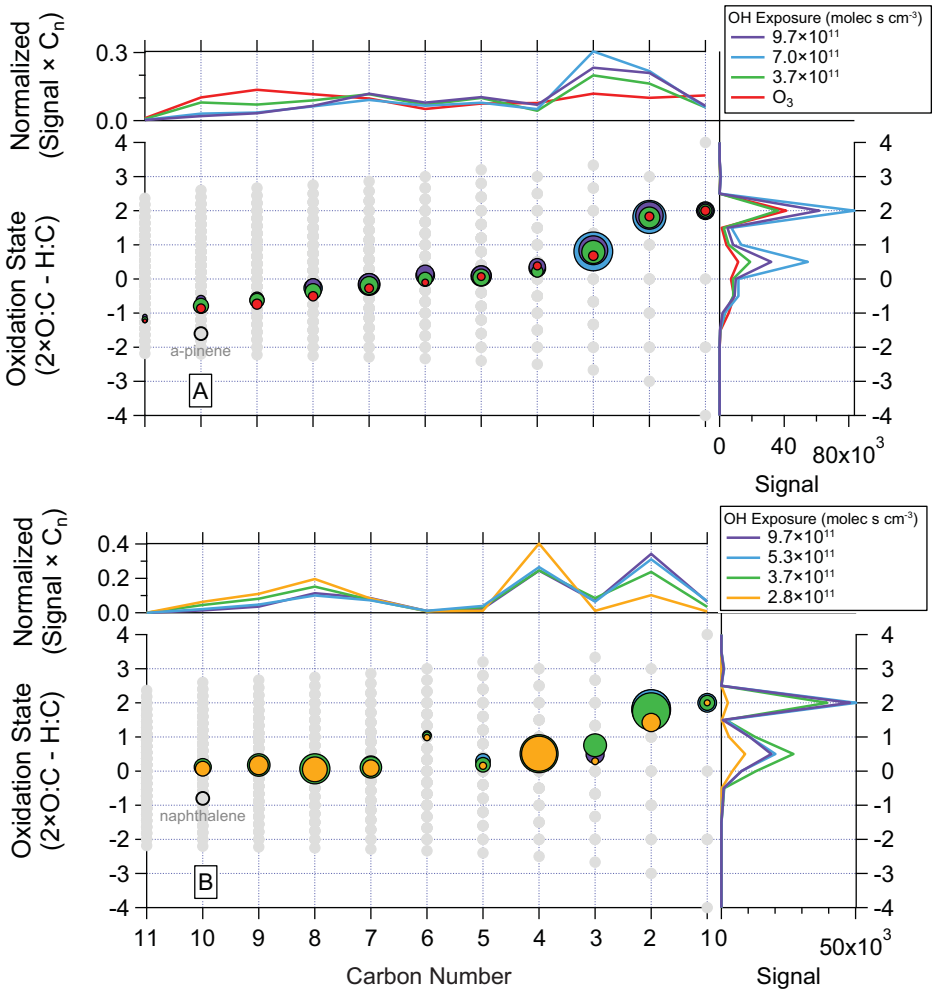

Figure 4. Kroll diagram for α-pinene **(a)** and naphthalene **(b)** oxidation experiments. The main panel displays the average OS_C per carbon number for each oxidation experiment. The area of the marker is proportional to the signal times the carbon number. The top panel plots the fraction of carbon-weighted signal at each carbon number. The right panel displays the signal distribution across oxidation state.

exposure. The fact that this decrease is directly correlated with an increase in the fraction of acids with $n_C < 4$ suggests that the $n_C < 4$ species are largely produced by fragmentation processes in which carbon–carbon bond cleavage occurs during oxidation of the $n_C = 8$ to 10 species.

Several other precursor-specific features are evident from Fig. 4. First, as is illustrated by the marker size in the main panel and curves in the right panel, CIMS signals peak at OH exposures of 3.7×10^{11} and 7.0×10^{11} molec s cm^{-3} for naphthalene and α-pinene oxidation products, respectively. Second, the carbon distribution of naphthalene oxidation products has negligible contributions from molecules with $n_C = 3$, 5, and 6. This is because naphthalene is unlikely to form pyruvic acid, an $n_C = 3$ acid with a methyl group, given naphthalene's aromatic structure. Additionally, naphthalene oxidation is unlikely to form acids with $n_C = 5$ or 6 because fragmentation of three or more carbon–carbon bonds is required.

3.4 Calculation of SOA mass from CIMS spectra

Spectra represented in Figs. 2–4 are for organic acids in the combined gas and particle phases. To estimate their relative contributions in each phase, we first calculated effective saturation concentrations (c^*) for each species shown in Fig. 3 using the algorithm described in Sect. 2.4. Table 2 lists examples of detected species from each precursor system and their corresponding c^* values. As shown, SIMPOL.1 estimates pinic acid ($C_9H_{14}O_4$) to have a $c^* = 3.68 \pm 8.47\,\mu g\,m^{-3}$ which is in good agreement with the $c^* = 5.34\,\mu g\,m^{-3}$ measured by Bilde and Pandis (2001). As shown in the Supplement and in Table 2, uncertainty in SIMPOL estimated vapor pressures increases with decreasing volatility.

To estimate the total mass concentration, M_i of each species i in $\mu g\,m^{-3}$ in a spectra, the formic acid sensitivity is applied to all ions using the following equation:

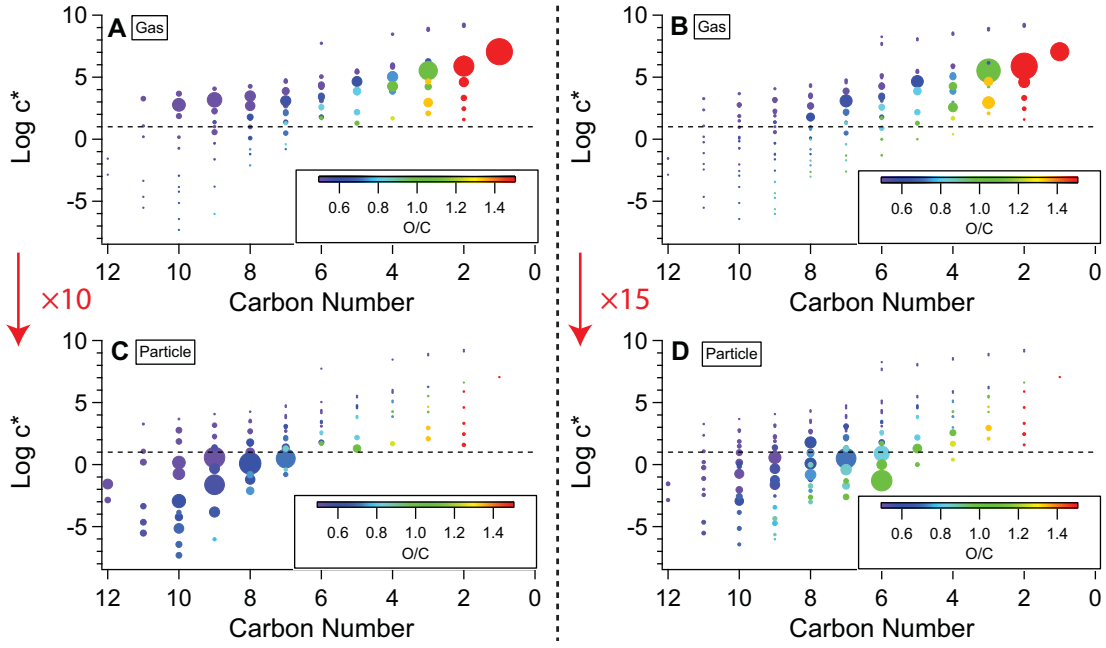

Figure 5. Estimated $\log c^*$ as a function of carbon number and O / C. **(a)** and **(c)** represent extracted gas and particle spectra of α-pinene ozonolysis (Expt 1), respectively, and **(b)** and **(d)** represent the same of α-pinene photooxidation at high OH exposures (Expt 7). Marker area is proportional to the fraction of mass in the depicted spectra. The factor and arrow in red represents the relative mass scale between gas and particle spectra. For example $\times 10$ between **(a)** and **(c)** indicate that markers of equal area represent the same fraction in each phase and 10 times more mass in the gas-phase spectrum.

$$M_i = \frac{\mathrm{MW}_i I_i}{RT S_{\mathrm{FA}}} \times 10^{-6}, \tag{12}$$

where I_i is the signal of corresponding ion i in Hz, S_{FA} is the formic acid sensitivity, MW_i is the molecular weight of species i, R is the ideal gas constant (8.21×10^{-5} atm m^3 mol^{-1} K^{-1}), and T is the temperature in Kelvin. The mass fraction of species i that partitions into the condensed phase is determined using Eq. (13) (Donahue et al., 2006):

$$\xi_i = \frac{1}{1 + \frac{c_i^*}{C_{\mathrm{OA}}}}, \tag{13}$$

where C_{OA} is the organic aerosol concentration. Here, instead of being a quantity that is solved for iteratively, we assume C_{OA} to take on decadal values of 1, 10 or 100 µg m^{-3} to determine how much of the measured spectra partitions into the condensed phase. The total mass estimated to be in the particle phase, C_{CIMS}, is then calculated as

$$C_{\mathrm{CIMS}} = \sum M_i \xi_i. \tag{14}$$

Application of Eqs. (12)–(14) allows for isolation of gas- and condensed-phase components of the CIMS spectra at a specific C_{OA}. Figure 5 plots c^* as a function of n_{C} for α-pinene ozonolysis and α-pinene photooxidation products (OH exposure $= 9.7 \times 10^{11}$ molec s cm^{-3}). Signals are apportioned into separate gas and particle-phase spectra assuming $C_{\mathrm{OA}} = 10$ µg m^{-3} which is representative of urban conditions (Zhang et al., 2007). Under these conditions, compounds with $c^* = 10$ µg m^{-3} will partition equally between the gas and particle phases. The factor and arrow in red represents the relative mass scale between gas and particle spectra. For example $\times 10$ between panels A and C indicate that markers of equal area represent 10 times more mass in the gas-phase spectrum. Figure 5 indicates that calculated c^* values decrease with increasing n_{C} and O / C ratio. Specifically, low-volatility $n_{\mathrm{C}} = 7$ to 10 compounds ($c^* = 1$ to 10^{-8} µg m^{-3}) dominate the particle-phase spectra while higher-volatility $n_{\mathrm{C}} = 1$ to 3 compounds ($c^* = 100$ to 10^6 µg m^{-3}) dominate the gas-phase spectra. Signals in both phases shift to lower n_{C} and higher O / C ratio with increasing OH exposure. An acid of significant importance in the particle phase at high OH exposures is $C_6H_8O_6$. Though modeled as a diacid, this species may be a $-CH_2$ homologue of the triacid MBTCA. In total, the modeled particle phase represents 10 and 7.0 % of the measured mass and 5 and 3.5 % of the measured ion signal for ozonolysis and high OH conditions, respectively. Figure S7 in the Supplement shows c^* as a function of n_{C} for naphthalene oxidation products; in general, similar trends are observed as in the α-pinene system.

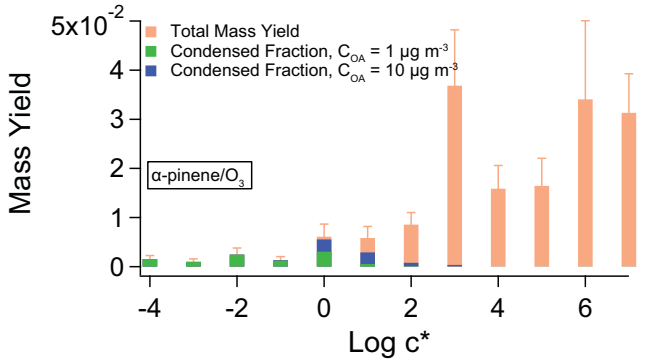

Figure 6. Estimated mass yield of compounds measured by the acetate-CIMS for α-pinene ozonolysis (Expt 1), binned by $\log c^*$. Colored in green is the fraction that would condense with $C_{OA} = 1\,\mu g\,m^{-3}$ and colored in blue is the additional mass that would condense with $C_{OA} = 10\,\mu g\,m^{-3}$. Error bars represent 1σ uncertainty from spectral variation, precursor concentration, and sensitivity

3.4.1 Derivation of acetate-CIMS volatility basis set and yields

Figure 6 shows the corresponding volatility basis set plot for α-pinene ozonolysis products measured with acetate-CIMS. Here, the calculated CIMS mass is normalized to the mass of α-pinene injected and plotted as a function of c^* (calculated c^* values are binned to the nearest c^* decade). The sum of the blue or green bars represents the aerosol mass fraction at $C_{OA} = 10$ and $C_{OA} = 1\,\mu g\,m^{-3}$, respectively. The c^* bins at the far right of the plot ($\log c^* = 6$ to 7) are dominated by formic, glyoxylic, and pyruvic acids which contribute 40 % of the total mass measured by the CIMS. Additionally, pinonic acid ($C_{10}H_{16}O_3$) and norpinonic acid ($C_9H_{14}O_3$) contribute significantly to the $\log c^* = 3$ bin. Error bars in Fig. 6 represent the combined 1σ uncertainty from spectra variation, sensitivity uncertainty, and precursor concentration uncertainty

Aerosol mass fractions (i.e., yields, ξ) were calculated for α-pinene experiments listed in Table 1 and are shown in Fig. 7 as a function of OH exposure. The ξ were calculated using particle-phase acetate-CIMS signals for decadal C_{OA} values of 1 to $100\,\mu g\,m^{-3}$:

$$\xi_{CIMS} = \frac{C_{CIMS}}{M_{pre}}, \quad (15)$$

where M_{pre} is the mass concentration of the injected aerosol precursor. The CIMS yields are compared to previously published yields determined from PAM experiments (Lambe et al., 2011a; Chen et al., 2013) and smog chamber experiments (Ng et al., 2006; Shilling et al., 2008; Eddingsaas et al., 2012). PAM yields as a function of OH exposure are represented by the gray shaded region. For α-pinene ozonolysis experiments conducted in the PAM, SOA yields, ξ_{SOA}, spanned from 11 to 24 %. These yields, applied to the α-pinene precursor concentrations used in this study, results in predicted SOA concentrations of 9 to $40\,\mu g\,m^{-3}$, corresponding to the CIMS yield curves with $C_{OA} = 10$ and $100\,\mu g\,m^{-3}$. For ozonolysis conditions, our estimate of SOA yields determined by the acetate-CIMS spectra, ξ_{CIMS} for 10 to $100\,\mu g\,m^{-3}$ of partitioning mass, range from about 2 ± 0.3 to 3 ± 0.7 %. Since acids are a subset of the entire SOA mass created, we would expect $\xi_{CIMS} \leq \xi_{SOA}$. Using a Micro-Orifice Volatilization Impactor (MOVI) inlet with an acetate-CIMS, Yatavelli et al. (2012) estimated 11–34 % of α-pinene ozonolysis SOA mass was acidic, in agreement with measurements by Yu et al. (1999). Using the acid yields for 10 to $100\,\mu g\,m^{-3}$ of partitioning mass and the range of SOA yields from PAM experiments, our calculations suggest that acids comprise 8–27 % of the measured mass of α-pinene ozonolysis SOA and are thereby consistent with the results of Yu et al. (1999) and Yatavelli et al. (2012). We also find that ξ_{CIMS}/ξ_{SOA} increases systematically with increasing exposure. This observation is consistent with previous studies demonstrating an increase in acid content of SOA, indicated by the increase in the fraction of m/z 44 (f_{44}), as a function of OH exposure (Lambe et al., 2011b) suggesting that acids are an important class of compounds in aged air masses (Ng et al., 2011). ξ_{CIMS} and ξ_{SOA} increase and subsequently decrease as a function of OH exposure. This trend is consistent with a transition from functionalization- to fragmentation-dominated reaction pathways (Kroll et al., 2009; Lambe et al., 2012) and supports our interpretation of $n_C = 7$ to 10 and $n_C < 4$ as tracers for functionalization and fragmentation processes, respectively.

Implicit in the calculation of the CIMS yield curves shown in Fig. 7 is the assumption that the total (sum of gas and particle phases) distribution of acids generated is only a function of OH exposure and is independent of the amount of hydrocarbon injected. In reality, variations in the amount of injected aerosol precursor can introduce non-linearity in the formation of product species, for example, through competition for oxidants or bimolecular reactions of radical products. We ignore such non-linearities here but note that they should be studied in the future.

Naphthalene CIMS yields range from 1 to 11 % with the maximum yield occurring at an OH exposure of 3.7×10^{11} molec s cm^{-3}, thus also exhibiting a transition from functionalization to fragmentation processes. Previous smog chamber studies have estimated that the acid yield of naphthalene under low-NO_x conditions is approximately 24 % of the SOA mass acidic in nature (Kautzman et al., 2009). Reasons for this discrepancy are unclear at present.

Error bars in Fig. 7 represent the combined uncertainty in sensitivity, spectral variation, estimated vapor pressure, and precursor concentration which varied from 11 to 37 % of the estimated yield. As was stated earlier, we use an average relative sensitivity for all acids based on the measured sensitivity of formic acid. While this may introduce significant error for individual species, it provides a practical way to estimate en-

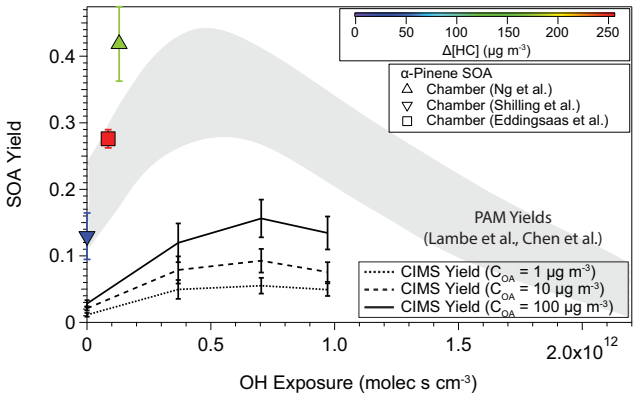

Figure 7. SOA yields estimated by the acetate-CIMS in this study and previously reported SOA yields from scanning mobility particle sizer (SMPS) measurements for α-pinene oxidation systems. The dotted black lines depict CIMS yields calculated for $C_{OA} = 1$, 10, and 100 $\mu g\,m^{-3}$. The gray shaded region represents the domain of yields determined from PAM experiments across OH exposure where the amount of α-pinene reacted ranged from 227 to 556 $\mu g\,m^{-3}$. Zero OH exposure corresponds to ozonolysis. Square and triangle points indicate yields determined from chamber experiments; their colors are indicative of the amount of α-pinene reacted. Error bars represent 1σ uncertainty from spectral variation, precursor concentration, sensitivity, and vapor pressure estimation.

semble properties. Its use for the acetate-CIMS may be particularly applicable since the acetate reagent scheme is primarily sensitive to acids. Based on previously reported sensitivities, we estimate an error of 60 % in the relative sensitivity of acids to formic acid. Aljawhary et al. (2013) measured the sensitivity of several different acids to acetate ionization, and found they were within a factor of 4. Of the acids measured, pinonic acid is the most relevant to our system and has a sensitivity approximately double that of formic acid. If this sensitivity is more representative of highly oxidized, lower-volatility compounds extracted from acetate-CIMS spectra, then the calculated ξ_{CIMS} is lower by roughly a factor of 1.5.

Another uncertainty involves the SIMPOL vapor pressure estimation method. Pankow and Asher (2008) report that calculated vapor pressures were typically within a factor of 2 of measured values. However, this variability is larger at low volatilities due to the lack of experimental vapor pressure measurements to constrain the parameterization. Compernolle et al. (2010) applied seven different vapor pressure estimation methods to a modeling study of SOA formation from α-pinene ozonolysis. They found that while there was general agreement for semi-volatile compounds, the vapor pressures estimated for low-volatility α-pinene acid tracers varied 3 orders of magnitude, leading to large differences in SOA yields. SIMPOL in particular tended to underestimate vapor pressures more than a similar method developed by (Capouet and Müller, 2006) due to the former's equal treatment of primary, secondary, and tertiary alcohols and lower volatilities given to carbon backbones and thus overestimating α-pinene ozonolysis yields in their model. At best, model simulations of α-pinene oxidation and SOA formation have agreed with experimental yields within a factor of 2 (Capouet et al., 2008). Although uncertainty in vapor pressure may be largest for the lowest volatility species, these species will completely partition into the condensed phase. It is the uncertainty in vapor pressure of compounds with c^* close to C_{OA} that will have the largest contribution to the error in the yield.

Recently, hydroperoxide moieties have been implicated in the composition of highly oxidized, extremely low-volatility organic compounds (ELVOC) (Ehn et al., 2014). In the functional group attribution method presented in Sect. 2.4, hydroperoxide moieties are indistinguishable from hydroxyl groups and one $-$OOH group would be attributed as two $-$OH groups. According to the SIMPOL model, hydroxy and hydroperoxide groups produce similar reductions in volatility ($b_{OH} = -2.23$ and $b_{OOH} = -2.49$ in Eq. 11) and thus the existence of hydroperoxide groups in detected molecules would lead to an underestimate in volatility and overestimate in acid yield.

Lastly, a potentially significant uncertainty is the estimation of the contribution of clustering in the high-resolution spectra. Here we set constraints on the ratio of cluster to molecular ion signals based on the assumption that the efficiency of clustering is constant for a given elemental composition. However, isomers may have different clustering efficiencies.

3.4.2 Comparison of particle-phase CIMS and Aerodyne AMS measurements

Figure 8 shows a Van Krevelen diagram of SOA species directly measured by the AMS and estimated from the acetate-CIMS for the oxidation of α-pinene and naphthalene. To facilitate this comparison, we calculated average O / C and H / C ratios of the particle-phase CIMS species (solid colored markers) for all experiments listed in Table 1 with exposure values similar to the published AMS data from Lambe et al. (2011b). Figure 8 shows that the O / C and H / C ratios measured by CIMS and AMS fall in the same region of the Van Krevelen diagram for α-pinene and naphthalene oxidation products. Additionally, the range of elemental ratios measured for the α-pinene system are consistent with the range observed by Aljawhary et al. (2013) in their experiments of WSOC formed from aqueous-phase α-pinene oxidation. This supports our interpretation that the low-volatility molecules measured by acetate-CIMS represent species contributing to SOA formation. However, we note that CIMS elemental ratios of α-pinene and naphthalene oxidation products span a smaller range of O / C than the AMS measurements conducted at similar exposures. One possible explanation is CIMS inlet losses of extremely low-volatility compounds; specifically, thermodenuder measurements have

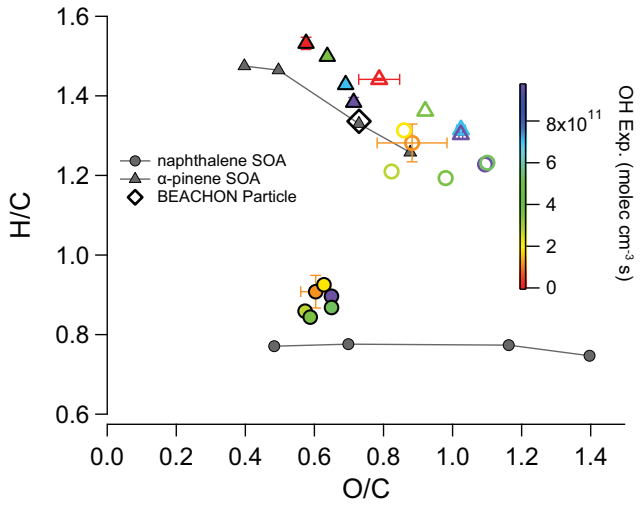

Figure 8. Average O / C and H / C ratios for extracted particle-phase (solid colored markers) and gas-phase (outlined colored markers) acetate-CIMS spectra (at $C_{OA} = 10\,\mu g\,m^{-3}$) as a function of OH exposure. Gray points represent AMS elemental ratios from Lambe et al. (2011a). Average particle-phase elemental ratios from the BEACHON-RoMBAS field campaign obtained from MOVI-HR-ToF-CIMS measurements are depicted by a black diamond (Yatavelli et al., 2014; Ortega et al., 2014). Error bars represent 1 standard deviation for multiple experiments.

shown that up to 30 % of particle-phase organic acid mass is not volatilized at 200 °C (Huffman et al., 2009). Another possibility is that highly functionalized organic acids may decompose in the inlet into products that are neither detected by the CIMS nor converted into smaller n_C acids (Yatavelli et al., 2014; Moldoveanu, 2010). Additionally, in the case of naphthalene, it may be difficult for oxidation products with acid groups to reach O / C values obtained in aerosol phase generated in the PAM at the highest OH exposures without extensive fragmentation.

Also shown in Fig. 8 are the average O / C and H / C ratios of the gas-phase CIMS species, illustrated by outlined colored markers. We observe much higher average O / C ratios for the estimated gas phase than the particle phase consistent with the production of small acids formed from the fragmentation of a larger carbon backbone. The H / C ratios of α-pinene gas-phase products are lower than those of the particle phase suggesting that the gas-phase acids might have more carbonyl groups and thus carbon with a higher oxidation state than carbon in the particle phase. In contrast, the H / C ratios of naphthalene gas-phase products are higher than those of the particle phase indicating that oxidation and fragmentation increase the oxidation state of carbon relative to carbon in aromatic rings. Particularly, the difference suggests that the particle phase is dominated by aromatic ring-retaining products while the gas phase is dominated by non-aromatic acid fragmentation products. The elemental ratios of the gas-phases products from both precursors display a convergence with increased OH exposure indicating the predominance of the same $n_C = 1$ to 4 acids, especially glyoxylic and glycolic acids.

Figure 8 also shows average O / C and H / C ratios of ambient organic aerosols measured with an acetate-MOVI-HR-ToF-CIMS during the Bio-hydro-atmosphere interactions of Energy, Aerosols, Carbon, H_2O, Organics and Nitrogen – Rocky Mountain Biogenic Aerosol Study (BEACHON-RoMBAS) field campaign (Yatavelli et al., 2014; Ortega et al., 2014). The BEACHON-RoMBAS measurements were obtained in a ponderosa pine forest and thus were influenced by emissions of biogenic compounds such as α-pinene. CIMS elemental ratios of highly oxidized α-pinene products produced in the PAM reactor agree with ambient measurements within 10 %. Interestingly, Yatavelli et al. (2014) were able to successfully model the partitioning of organic acids in bulk as alkanoic acids with excess oxygen in the form of hydroxyl groups, each lowering the vapor pressure by SIMPOL estimated factors. Our method uses the measured ion formulas to constrain the double bond equivalency and limit additional oxygen functional groups. These similarities suggest that the volatility estimation algorithm successfully captures atmospheric photochemistry of atmospherically relevant SOA precursors, and that our results can be used to interpret ambient measurements in different source regions.

4 Discussion and conclusions

The gas-phase SOA precursors for O_3 and OH oxidation of α-pinene and naphthalene were measured for the first time using a PAM flow reactor and an HR-ToF-CIMS with acetate reagent ion chemistry. The measured organic acid distributions exhibited similarities to gas-phase measurements from previous environmental chamber studies (Yu et al., 1999; Claeys et al., 2013; Kautzman et al., 2009). These measurements extend the previous measurements to higher OH exposures and include observations of several previously unidentified organic acids, particularly for naphthalene. Particularly, they illustrate the concurrent functionalization and fragmentation processes occurring in the gas-phase yielding high and low carbon number acids, the latter dominating the spectra.

In addition, we have presented an approach to estimate the vapor pressures and gas-to-particle partitioning of select organic compounds using HR-ToF-CIMS gas-phase measurements in combination with an algorithm based on the SIMPOL group contribution parameterization method introduced by Pankow and Asher (2008). Previous applications of SIMPOL attempted to use Aerodyne AMS measurements to calculate vapor pressures of organic compounds from their measured elemental ratios (O / C and H / C). However, since functional group information is not available from AMS, spectra simplifying assumptions are required which can introduce additional uncertainty (e.g., Donahue et al., 2011). Most recently Yatavelli et al. (2014) applied SIMPOL to

MOVI-HR-ToF-CIMS spectra using the acetate reagent ion. They were able to capture the bulk partitioning of species by carbon number, by modeling detected compounds such as alkanoic acids, and adding the remainder of oxygens in the form of different functional groups with hydroxyl groups giving the best agreement. Our approach builds on these studies by incorporating the DBE content of the measured species towards the goal of explicit characterization of oxygen-containing functional groups. This analysis is made possible by the high-mass resolution of the TOFWERK HTOF which can resolve the chemical formulas of detected ions.

Our model performs well in predicting the acid contribution to SOA formed from α-pinene ozonolysis compared to previous measurements (Yu et al., 1999; Yatavelli et al., 2012) and to our knowledge, this is the first attempt to estimate the mass of a class of compounds from CIMS spectra using a group contribution model. Semi-explicit model simulations of α-pinene oxidation and SOA formation have agreed with experimental yields within a factor of 2 (Capouet et al., 2008) while models with more degrees of freedom can be tuned to have even greater accuracies (Cappa and Wilson, 2012). Although we use SIMPOL parameterizations as a case study, our method can be adapted for the use of different vapor pressure formulation methods (Nannoolal et al., 2004, 2008; Hilal et al., 1994; Moller et al., 2008). The advantage of SIMPOL is that only functional group composition and carbon number information are needed in the parameterization. Various studies have compared vapor pressure models and have shown that volatility estimation, and thus aerosol formation, is highly sensitive to model choice (Compernolle et al., 2010; Barley and McFiggans, 2010; Clegg et al., 2008). Additionally, different reagent chemistries (e.g., $(H_2O)_nH^+$, I^-, NO_3^-) can and should be tested with our model to validate its effectiveness on different classes of compounds. For instance, iodide spectra may be more easily analyzed since its clusters do not contain carbon

With recent advances in CIMS measurement techniques that allow for separation of gas- and particle-phase analytes (Yatavelli and Thornton, 2010; Lopez-Hilfiker et al., 2014), uncertainties in the quantification of unknown organics will have to be addressed. For instance, epoxides and peroxides have been implicated in SOA formation in low-NO_x isoprene systems. Thus, our model needs to be tested against additional SOA systems and subsequently refined. In our study we assume that all detected species have the same ionization efficiency, relative to formic acid. While recent studies suggest that this approximation may be acceptable (Aljawhary et al., 2013) more data are needed to constrain acetate ionization efficiencies across carbon number and oxidation state. Additionally, the variables that control clustering, including operational voltages, IMR pressure, and reagent ion and neutral concentrations in the IMR, need to be explored. Use of isotopically labeled reagent ions may aid in this these investigations.

The Supplement related to this article is available online at doi:10.5194/amt-8-1-2015-supplement.

Acknowledgements. This work was supported by the Atmospheric Chemistry Program of the National Science Foundation, grants no. AGS-1244918 and no. ATM-0854916 to Boston College and no. AGS-1244999 and no. AGS-0904292 to Aerodyne Research, Inc. We would also like to acknowledge DOE SBIR grant no. DE-SC0004577 and Office of Science (BER), Department of Energy (Atmospheric Systems Research) grants no. DE-SC0006980 and DE-FG02-05ER63995. The authors would like to thank William Brune for canisters of α-pinene and Erika Hale at the University of Texas for assistance in error calculations.

Edited by: P. Herckes

References

Aiken, A. C., DeCarlo, P. F., and Jimenez, J. L.: Elemental Analysis of Organic Species with Electron Ionization High-Resolution Mass Spectrometry, Anal. Chem., 79, 8350–8358, doi:10.1021/ac071150w, 2007.

Aiken, A. C., DeCarlo, P. F., Kroll, J. H., Worsnop, D. R., Huffman, J. A., Docherty, K. S., Ulbrich, I. M., Mohr, C., Kimmel, J. R., Sueper, D., Sun, Y., Zhang, Q., Trimborn, A., Northway, M., Ziemann, P. J., Canagaratna, M. R., Onasch, T. B., Alfarra, M. R., Prevot, A. S. H., Dommen, J., Duplissy, J., Metzger, A., Baltensperger, U., and Jimenez, J. L.: O/C and OM/OC Ratios of Primary, Secondary, and Ambient Organic Aerosols with High-Resolution Time-of-Flight Aerosol Mass Spectrometry, Environ. Sci. Technol., 42, 4478–4485, doi:10.1021/es703009q, 2008.

Aljawhary, D., Lee, A. K. Y., and Abbatt, J. P. D.: High-resolution chemical ionization mass spectrometry (ToF-CIMS): application to study SOA composition and processing, Atmos. Meas. Tech., 6, 3211–3224, doi:10.5194/amt-6-3211-2013, 2013.

Atkinson, R. and Aschmann, S. M.: Kinetics of the reactions of naphthalene, 2-methylnaphthalene, and 2,3-dimethylnaphthalene with OH radicals and with O_3 at 295 ± 1 K, Int. J. Chem. Kinet., 18, 569–573, doi:10.1002/kin.550180507, 1986.

Barley, M. H. and McFiggans, G.: The critical assessment of vapour pressure estimation methods for use in modelling the formation of atmospheric organic aerosol, Atmos. Chem. Phys., 10, 749–767, doi:10.5194/acp-10-749-2010, 2010.

Bertram, T. H., Kimmel, J. R., Crisp, T. A., Ryder, O. S., Yatavelli, R. L. N., Thornton, J. A., Cubison, M. J., Gonin, M., and Worsnop, D. R.: A field-deployable, chemical ionization time-of-flight mass spectrometer, Atmos. Meas. Tech., 4, 1471–1479, doi:10.5194/amt-4-1471-2011, 2011.

Bilde, M. and Pandis, S. N.: Evaporation Rates and Vapor Pressures of Individual Aerosol Species Formed in the Atmospheric Oxidation of alpha- and beta-Pinene, Environ. Sci. Technol., 35, 3344–3349, doi:10.1021/es001946b, 2001.

Canagaratna, M. R., Jayne, J. T., Jimenez, J. L., Allan, J. D., Alfarra, M. R., Zhang, Q., Onasch, T. B., Drewnick, F., Coe, H., Middlebrook, A., Delia, A., Williams, L. R., Trimborn, A. M., Northway, M. J., DeCarlo, P. F., Kolb, C. E., Davidovits, P., and

Worsnop, D. R.: Chemical and microphysical characterization of ambient aerosols with the aerodyne aerosol mass spectrometer, Mass Spectrom. Rev., 26, 185–222, doi:10.1002/mas.20115, 2007.

Capouet, M. and Müller, J.-F.: A group contribution method for estimating the vapour pressures of α-pinene oxidation products, Atmos. Chem. Phys., 6, 1455–1467, doi:10.5194/acp-6-1455-2006, 2006.

Capouet, M., Müller, J. F., Ceulemans, K., Compernolle, S., Vereecken, L., and Peeters, J.: Modeling aerosol formation in alpha-pinene photo-oxidation experiments, J. Geophys. Res.-Atmos., 113, D02308, doi:10.1029/2007JD008995, 2008.

Cappa, C. D.: A model of aerosol evaporation kinetics in a thermodenuder, Atmos. Meas. Tech., 3, 579–592, doi:10.5194/amt-3-579-2010, 2010.

Cappa, C. D. and Jimenez, J. L.: Quantitative estimates of the volatility of ambient organic aerosol, Atmos. Chem. Phys., 10, 5409–5424, doi:10.5194/acp-10-5409-2010, 2010.

Cappa, C. D. and Wilson, K. R.: Multi-generation gas-phase oxidation, equilibrium partitioning, and the formation and evolution of secondary organic aerosol, Atmos. Chem. Phys., 12, 9505–9528, doi:10.5194/acp-12-9505-2012, 2012.

Chan, A. W. H., Kautzman, K. E., Chhabra, P. S., Surratt, J. D., Chan, M. N., Crounse, J. D., Kürten, A., Wennberg, P. O., Flagan, R. C., and Seinfeld, J. H.: Secondary organic aerosol formation from photooxidation of naphthalene and alkylnaphthalenes: implications for oxidation of intermediate volatility organic compounds (IVOCs), Atmos. Chem. Phys., 9, 3049–3060, doi:10.5194/acp-9-3049-2009, 2009.

Chen, S., Brune, W. H., Lambe, A. T., Davidovits, P., and Onasch, T. B.: Modeling organic aerosol from the oxidation of α-pinene in a Potential Aerosol Mass (PAM) chamber, Atmos. Chem. Phys., 13, 5017–5031, doi:10.5194/acp-13-5017-2013, 2013.

Chhabra, P. S., Ng, N. L., Canagaratna, M. R., Corrigan, A. L., Russell, L. M., Worsnop, D. R., Flagan, R. C., and Seinfeld, J. H.: Elemental composition and oxidation of chamber organic aerosol, Atmos. Chem. Phys., 11, 8827–8845, doi:10.5194/acp-11-8827-2011, 2011.

Claeys, M., Szmigielski, R., Vermeylen, R., Wang, W., Shalamzari, M., and Maenhaut, W.: Tracers for Biogenic Secondary Organic Aerosol from alpha-Pinene and Related Monoterpenes: An Overview, book section 18, 227–238, NATO Science for Peace and Security Series C: Environmental Security, Springer Netherlands, doi:10.1007/978-94-007-5034-0_18, 2013.

Clegg, S. L., Kleeman, M. J., Griffin, R. J., and Seinfeld, J. H.: Effects of uncertainties in the thermodynamic properties of aerosol components in an air quality model – Part 2: Predictions of the vapour pressures of organic compounds, Atmos. Chem. Phys., 8, 1087–1103, doi:10.5194/acp-8-1087-2008, 2008.

Compernolle, S., Ceulemans, K., and Müller, J.-F.: Technical Note: Vapor pressure estimation methods applied to secondary organic aerosol constituents from α-pinene oxidation: an intercomparison study, Atmos. Chem. Phys., 10, 6271–6282, doi:10.5194/acp-10-6271-2010, 2010.

Daumit, K. E., Kessler, S. H., and Kroll, J. H.: Average chemical properties and potential formation pathways of highly oxidized organic aerosol, Faraday Discuss., 165, 181–202, doi:10.1039/C3FD00045A, 2013.

DeCarlo, P. F., Kimmel, J. R., Trimborn, A., Northway, M. J., Jayne, J. T., Aiken, A. C., Gonin, M., Fuhrer, K., Horvath, T., Docherty, K. S., Worsnop, D. R., and Jimenez, J. L.: Field-Deployable, High-Resolution, Time-of-Flight Aerosol Mass Spectrometer, Anal. Chem., 78, 8281–8289, doi:10.1021/ac061249n, 2006.

Donahue, N. M., Robinson, A. L., Stanier, C. O., and Pandis, S. N.: Coupled Partitioning, Dilution, and Chemical Aging of Semivolatile Organics, Environ. Sci. Technol., 40, 2635–2643, doi:10.1021/es052297c, 2006.

Donahue, N. M., Epstein, S. A., Pandis, S. N., and Robinson, A. L.: A two-dimensional volatility basis set: 1. organic-aerosol mixing thermodynamics, Atmos. Chem. Phys., 11, 3303–3318, doi:10.5194/acp-11-3303-2011, 2011.

Dzepina, K., Cappa, C. D., Volkamer, R. M., Madronich, S., DeCarlo, P. F., Zaveri, R. A., and Jimenez, J. L.: Modeling the Multiday Evolution and Aging of Secondary Organic Aerosol During MILAGRO 2006, Environ. Sci. Technol., 45, 3496–3503, doi:10.1021/es103186f, 2011.

Eddingsaas, N. C., Loza, C. L., Yee, L. D., Chan, M., Schilling, K. A., Chhabra, P. S., Seinfeld, J. H., and Wennberg, P. O.: α-pinene photooxidation under controlled chemical conditions – Part 2: SOA yield and composition in low- and high-NO_x environments, Atmos. Chem. Phys., 12, 7413–7427, doi:10.5194/acp-12-7413-2012, 2012.

Ehn, M., Kleist, E., Junninen, H., Petäjä, T., Lönn, G., Schobesberger, S., Dal Maso, M., Trimborn, A., Kulmala, M., Worsnop, D. R., Wahner, A., Wildt, J., and Mentel, Th. F.: Gas phase formation of extremely oxidized pinene reaction products in chamber and ambient air, Atmos. Chem. Phys., 12, 5113–5127, doi:10.5194/acp-12-5113-2012, 2012.

Ehn, M., Thornton, J. A., Kleist, E., Sipila, M., Junninen, H., Pullinen, I., Springer, M., Rubach, F., Tillmann, R., Lee, B., Lopez-Hilfiker, F., Andres, S., Acir, I.-H., Rissanen, M., Jokinen, T., Schobesberger, S., Kangasluoma, J., Kontkanen, J., Nieminen, T., Kurten, T., Nielsen, L. B., Jorgensen, S., Kjaergaard, H. G., Canagaratna, M., Maso, M. D., Berndt, T., Petaja, T., Wahner, A., Kerminen, V.-M., Kulmala, M., Worsnop, D. R., Wildt, J., and Mentel, T. F.: A large source of low-volatility secondary organic aerosol, Nature, 506, 476–479, doi:10.1038/nature13032, 2014.

Ervens, B., Turpin, B. J., and Weber, R. J.: Secondary organic aerosol formation in cloud droplets and aqueous particles (aqSOA): a review of laboratory, field and model studies, Atmos. Chem. Phys., 11, 11069–11102, doi:10.5194/acp-11-11069-2011, 2011.

Farmer, D. K., Matsunaga, A., Docherty, K. S., Surratt, J. D., Seinfeld, J. H., Ziemann, P. J., and Jimenez, J. L.: Response of an aerosol mass spectrometer to organonitrates and organosulfates and implications for atmospheric chemistry, P. Natl. Acad. Sci., 107, 6670–6675, doi:10.1073/pnas.0912340107, 2010.

Fu, T.-M., Jacob, D. J., Wittrock, F., Burrows, J. P., Vrekoussis, M., and Henze, D. K.: Global budgets of atmospheric glyoxal and methylglyoxal, and implications for formation of secondary organic aerosols, J. Geophys. Res.-Atmos., 113, D15303, doi:10.1029/2007JD009505, 2008.

Galloway, M. M., Chhabra, P. S., Chan, A. W. H., Surratt, J. D., Flagan, R. C., Seinfeld, J. H., and Keutsch, F. N.: Glyoxal uptake on ammonium sulphate seed aerosol: reaction products and reversibility of uptake under dark and irradiated conditions, At-

mos. Chem. Phys., 9, 3331–3345, doi:10.5194/acp-9-3331-2009, 2009.

Goldstein, A. H. and Galbally, I. E.: Known and Unexplored Organic Constituents in the Earth's Atmosphere, Environ. Sci. Technol., 41, 1514–1521, doi:10.1021/es072476p, 2007.

Hallquist, M., Wenger, J. C., Baltensperger, U., Rudich, Y., Simpson, D., Claeys, M., Dommen, J., Donahue, N. M., George, C., Goldstein, A. H., Hamilton, J. F., Herrmann, H., Hoffmann, T., Iinuma, Y., Jang, M., Jenkin, M. E., Jimenez, J. L., Kiendler-Scharr, A., Maenhaut, W., McFiggans, G., Mentel, Th. F., Monod, A., Prévôt, A. S. H., Seinfeld, J. H., Surratt, J. D., Szmigielski, R., and Wildt, J.: The formation, properties and impact of secondary organic aerosol: current and emerging issues, Atmos. Chem. Phys., 9, 5155–5236, doi:10.5194/acp-9-5155-2009, 2009.

Heald, C. L., Kroll, J. H., Jimenez, J. L., Docherty, K. S., DeCarlo, P. F., Aiken, A. C., Chen, Q., Martin, S. T., Farmer, D. K., and Artaxo, P.: A simplified description of the evolution of organic aerosol composition in the atmosphere, Geophys. Res. Lett., 37, L08803, doi:10.1029/2010GL042737, 2010.

Herndon, S. C., Zahniser, M. S., Nelson, D. D., Shorter, J., McManus, J. B., Jiménez, R., Warneke, C., and de Gouw, J. A.: Airborne measurements of HCHO and HCOOH during the New England Air Quality Study 2004 using a pulsed quantum cascade laser spectrometer, J. Geophys. Res.-Atmos., 112, D10S03, doi:10.1029/2006JD007600, 2007.

Hilal, S. H., Carreira, A., and Karikhoff, S. W.: Estimation of chemical reactivity parameters and physical properties of organic molecules using SPARC, book section 9, 291–353, Elsevier, 1st Edn., 1994.

Huffman, J. A., Docherty, K. S., Aiken, A. C., Cubison, M. J., Ulbrich, I. M., DeCarlo, P. F., Sueper, D., Jayne, J. T., Worsnop, D. R., Ziemann, P. J., and Jimenez, J. L.: Chemically-resolved aerosol volatility measurements from two megacity field studies, Atmos. Chem. Phys., 9, 7161–7182, doi:10.5194/acp-9-7161-2009, 2009.

Jayne, J. T., Leard, D. C., Zhang, X., Davidovits, P., Smith, K. A., Kolb, C. E., and Worsnop, D. R.: Development of an Aerosol Mass Spectrometer for Size and Composition Analysis of Submicron Particles, Aerosol Sci. Technol., 33, 49–70, doi:10.1080/027868200410840, 2000.

Jimenez, J. L., Canagaratna, M. R., Donahue, N. M., Prevot, A. S. H., Zhang, Q., Kroll, J. H., DeCarlo, P. F., Allan, J. D., Coe, H., Ng, N. L., Aiken, A. C., Docherty, K. S., Ulbrich, I. M., Grieshop, A. P., Robinson, A. L., Duplissy, J., Smith, J. D., Wilson, K. R., Lanz, V. A., Hueglin, C., Sun, Y. L., Tian, J., Laaksonen, A., Raatikainen, T., Rautiainen, J., Vaattovaara, P., Ehn, M., Kulmala, M., Tomlinson, J. M., Collins, D. R., Cubison, M. J., E., Dunlea, J., Huffman, J. A., Onasch, T. B., Alfarra, M. R., Williams, P. I., Bower, K., Kondo, Y., Schneider, J., Drewnick, F., Borrmann, S., Weimer, S., Demerjian, K., Salcedo, D., Cottrell, L., Griffin, R., Takami, A., Miyoshi, T., Hatakeyama, S., Shimono, A., Sun, J. Y., Zhang, Y. M., Dzepina, K., Kimmel, J. R., Sueper, D., Jayne, J. T., Herndon, S. C., Trimborn, A. M., Williams, L. R., Wood, E. C., Middlebrook, A. M., Kolb, C. E., Baltensperger, U., and Worsnop, D. R.: Evolution of Organic Aerosols in the Atmosphere, Science, 326, 1525–1529, doi:10.1126/science.1180353, 2009.

Kang, E., Root, M. J., Toohey, D. W., and Brune, W. H.: Introducing the concept of Potential Aerosol Mass (PAM), Atmos. Chem. Phys., 7, 5727–5744, doi:10.5194/acp-7-5727-2007, 2007.

Kautzman, K. E., Surratt, J. D., Chan, M. N., Chan, A. W. H., Hersey, S. P., Chhabra, P. S., Dalleska, N. F., Wennberg, P. O., Flagan, R. C., and Seinfeld, J. H.: Chemical Composition of Gas- and Aerosol-Phase Products from the Photooxidation of Naphthalene, J. Phys. Chem. A, 114, 913–934, doi:10.1021/jp908530s, 2009.

Kessler, S. H., Smith, J. D., Che, D. L., Worsnop, D. R., Wilson, K. R., and Kroll, J. H.: Chemical Sinks of Organic Aerosol: Kinetics and Products of the Heterogeneous Oxidation of Erythritol and Levoglucosan, Environ. Sci. Technol., 44, 7005–7010, doi:10.1021/es101465m, 2010.

Kessler, S. H., Nah, T., Daumit, K. E., Smith, J. D., Leone, S. R., Kolb, C. E., Worsnop, D. R., Wilson, K. R., and Kroll, J. H.: OH-Initiated Heterogeneous Aging of Highly Oxidized Organic Aerosol, J. Phys. Chem. A, 116, 6358–6365, doi:10.1021/jp212131m, 2012.

Kroll, J. H. and Seinfeld, J. H.: Chemistry of secondary organic aerosol: Formation and evolution of low-volatility organics in the atmosphere, Atmos. Environ., 42, 3593–3624, doi:10.1016/j.atmosenv.2008.01.003, 2008.

Kroll, J. H., Smith, J. D., Che, D. L., Kessler, S. H., Worsnop, D. R., and Wilson, K. R.: Measurement of fragmentation and functionalization pathways in the heterogeneous oxidation of oxidized organic aerosol, Phys. Chem. Chem. Phys., 11, 8005–8014, doi:10.1039/B905289E, 2009.

Kroll, J. H., Donahue, N. M., Jimenez, J. L., Kessler, S. H., Canagaratna, M. R., Wilson, K. R., Altieri, K. E., Mazzoleni, L. R., Wozniak, A. S., Bluhm, H., Mysak, E. R., Smith, J. D., Kolb, C. E., and Worsnop, D. R.: Carbon oxidation state as a metric for describing the chemistry of atmospheric organic aerosol, Nat. Chem., 3, 133–139, doi:10.1038/nchem.948, 2011.

Kundu, S., Fisseha, R., Putman, A. L., Rahn, T. A., and Mazzoleni, L. R.: High molecular weight SOA formation during limonene ozonolysis: insights from ultrahigh-resolution FT-ICR mass spectrometry characterization, Atmos. Chem. Phys., 12, 5523–5536, doi:10.5194/acp-12-5523-2012, 2012.

Lambe, A. T., Ahern, A. T., Williams, L. R., Slowik, J. G., Wong, J. P. S., Abbatt, J. P. D., Brune, W. H., Ng, N. L., Wright, J. P., Croasdale, D. R., Worsnop, D. R., Davidovits, P., and Onasch, T. B.: Characterization of aerosol photooxidation flow reactors: heterogeneous oxidation, secondary organic aerosol formation and cloud condensation nuclei activity measurements, Atmos. Meas. Tech., 4, 445–461, doi:10.5194/amt-4-445-2011, 2011a.

Lambe, A. T., Onasch, T. B., Massoli, P., Croasdale, D. R., Wright, J. P., Ahern, A. T., Williams, L. R., Worsnop, D. R., Brune, W. H., and Davidovits, P.: Laboratory studies of the chemical composition and cloud condensation nuclei (CCN) activity of secondary organic aerosol (SOA) and oxidized primary organic aerosol (OPOA), Atmos. Chem. Phys., 11, 8913–8928, doi:10.5194/acp-11-8913-2011, 2011b.

Lambe, A. T., Onasch, T. B., Croasdale, D. R., Wright, J. P., Martin, A. T., Franklin, J. P., Massoli, P., Kroll, J. H., Canagaratna, M. R., Brune, W. H., Worsnop, D. R., and Davidovits, P.: Transitions from Functionalization to Fragmentation Reactions of Laboratory Secondary Organic Aerosol (SOA) Generated from the

OH Oxidation of Alkane Precursors, Environ. Sci. Technol., 46, 5430–5437, doi:10.1021/es300274t, 2012.

Laskin, A., Laskin, J., and Nizkorodov, S. A.: Mass spectrometric approaches for chemical characterisation of atmospheric aerosols: critical review of the most recent advances, Environ. Chem., 9, 163–189, doi:10.1071/EN12052, 2012.

Lee, A., Goldstein, A. H., Keywood, M. D., Gao, S., Varutbangkul, V., Bahreini, R., Ng, N. L., Flagan, R. C., and Seinfeld, J. H.: Gas-phase products and secondary aerosol yields from the ozonolysis of ten different terpenes, J. Geophys. Res.-Atmos., 111, D07302, doi:10.1029/2005JD006437, 2006a.

Lee, A., Goldstein, A. H., Kroll, J. H., Ng, N. L., Varutbangkul, V., Flagan, R. C., and Seinfeld, J. H.: Gas-phase products and secondary aerosol yields from the photooxidation of 16 different terpenes, J. Geophys. Res.-Atmos., 111, D17305, doi:10.1029/2006JD007050, 2006b.

Librando, V. and Tringali, G.: Atmospheric fate of OH initiated oxidation of terpenes. Reaction mechanism of alpha-pinene degradation and secondary organic aerosol formation, J. Environ. Manage., 75, 275–282, doi:10.1016/j.jenvman.2005.01.001, 2005.

Lim, Y. B., Tan, Y., Perri, M. J., Seitzinger, S. P., and Turpin, B. J.: Aqueous chemistry and its role in secondary organic aerosol (SOA) formation, Atmos. Chem. Phys., 10, 10521–10539, doi:10.5194/acp-10-10521-2010, 2010.

Lopez-Hilfiker, F. D., Mohr, C., Ehn, M., Rubach, F., Kleist, E., Wildt, J., Mentel, Th. F., Lutz, A., Hallquist, M., Worsnop, D., and Thornton, J. A.: A novel method for online analysis of gas and particle composition: description and evaluation of a Filter Inlet for Gases and AEROsols (FIGAERO), Atmos. Meas. Tech., 7, 983–1001, doi:10.5194/amt-7-983-2014, 2014.

Mao, J., Ren, X., Brune, W. H., Olson, J. R., Crawford, J. H., Fried, A., Huey, L. G., Cohen, R. C., Heikes, B., Singh, H. B., Blake, D. R., Sachse, G. W., Diskin, G. S., Hall, S. R., and Shetter, R. E.: Airborne measurement of OH reactivity during INTEX-B, Atmos. Chem. Phys., 9, 163–173, doi:10.5194/acp-9-163-2009, 2009.

Mazzoleni, L. R., Ehrmann, B. M., Shen, X., Marshall, A. G., and Collett, J. L.: Water-Soluble Atmospheric Organic Matter in Fog: Exact Masses and Chemical Formula Identification by Ultrahigh-Resolution Fourier Transform Ion Cyclotron Resonance Mass Spectrometry, Environ. Sci. Technol., 44, 3690–3697, doi:10.1021/es903409k, 2010.

Mohr, C., Lopez-Hilfiker, F. D., Zotter, P., Prévôt, A. S. H., Xu, L., Ng, N. L., Herndon, S. C., Williams, L. R., Franklin, J. P., Zahniser, M. S., Worsnop, D. R., Knighton, W. B., Aiken, A. C., Gorkowski, K. J., Dubey, M. K., Allan, J. D., and Thornton, J. A.: Contribution of Nitrated Phenols to Wood Burning Brown Carbon Light Absorption in Detling, United Kingdom during Winter Time, Environ. Sci. Technol., 47, 6316–6324, doi:10.1021/es400683v, 2013.

Moldoveanu, S. C.: Pyrolysis of Carboxylic Acids, Vol. 28 of Techniques and Instrumentation in Analytical Chemistry, book section 17, 471–526, Elsevier, doi:10.1016/S0167-9244(09)02817-0, 2010.

Moller, B., Rarey, J., and Ramjugernath, D.: Estimation of the vapour pressure of non-electrolyte organic compounds via group contributions and group interactions, J. Mol. Liq., 143, 52–63, doi:10.1016/j.molliq.2008.04.020, 2008.

Nannoolal, Y., Rarey, J., Ramjugernath, D., and Cordes, W.: Estimation of pure component properties: Part 1. Estimation of the normal boiling point of non-electrolyte organic compounds via group contributions and group interactions, Fluid Phase Equilibr., 226, 45–63, doi:10.1016/j.fluid.2004.09.001, 2004.

Nannoolal, Y., Rarey, J., and Ramjugernath, D.: Estimation of pure component properties: Part 3. Estimation of the vapor pressure of non-electrolyte organic compounds via group contributions and group interactions, Fluid Phase Equilibr., 269, 117–133, doi:10.1016/j.fluid.2008.04.020, 2008.

Ng, N. L., Kroll, J. H., Keywood, M. D., Bahreini, R., Varutbangkul, V., Flagan, R. C., Seinfeld, J. H., Lee, A., and Goldstein, A. H.: Contribution of First- versus Second-Generation Products to Secondary Organic Aerosols Formed in the Oxidation of Biogenic Hydrocarbons, Environ. Sci. Technol., 40, 2283–2297, doi:10.1021/es052269u, 2006.

Ng, N. L., Canagaratna, M. R., Jimenez, J. L., Chhabra, P. S., Seinfeld, J. H., and Worsnop, D. R.: Changes in organic aerosol composition with aging inferred from aerosol mass spectra, Atmos. Chem. Phys., 11, 6465–6474, doi:10.5194/acp-11-6465-2011, 2011.

Nishino, N., Arey, J., and Atkinson, R.: Yields of Glyoxal and Ring-Cleavage Co-Products from the OH Radical-Initiated Reactions of Naphthalene and Selected Alkylnaphthalenes, Environ. Sci. Technol., 43, 8554–8560, doi:10.1021/es902018v, 2009.

Orlando, J. J., Nozière, B., Tyndall, G. S., Orzechowska, G. E., Paulson, S. E., and Rudich, Y.: Product studies of the OH- and ozone-initiated oxidation of some monoterpenes, J. Geophys. Res.-Atmos., 105, 11561–11572, doi:10.1029/2000JD900005, 2000.

Ortega, J., Turnipseed, A., Guenther, A. B., Karl, T. G., Day, D. A., Gochis, D., Huffman, J. A., Prenni, A. J., Levin, E. J. T., Kreidenweis, S. M., DeMott, P. J., Tobo, Y., Patton, E. G., Hodzic, A., Cui, Y. Y., Harley, P. C., Hornbrook, R. S., Apel, E. C., Monson, R. K., Eller, A. S. D., Greenberg, J. P., Barth, M. C., Campuzano-Jost, P., Palm, B. B., Jimenez, J. L., Aiken, A. C., Dubey, M. K., Geron, C., Offenberg, J., Ryan, M. G., Fornwalt, P. J., Pryor, S. C., Keutsch, F. N., DiGangi, J. P., Chan, A. W. H., Goldstein, A. H., Wolfe, G. M., Kim, S., Kaser, L., Schnitzhofer, R., Hansel, A., Cantrell, C. A., Mauldin, R. L., and Smith, J. N.: Overview of the Manitou Experimental Forest Observatory: site description and selected science results from 2008 to 2013, Atmos. Chem. Phys., 14, 6345–6367, doi:10.5194/acp-14-6345-2014, 2014.

Pankow, J. F. and Asher, W. E.: SIMPOL.1: a simple group contribution method for predicting vapor pressures and enthalpies of vaporization of multifunctional organic compounds, Atmos. Chem. Phys., 8, 2773–2796, doi:10.5194/acp-8-2773-2008, 2008.

Putman, A. L., Offenberg, J. H., Fisseha, R., Kundu, S., Rahn, T. A., and Mazzoleni, L. R.: Ultrahigh-resolution FT-ICR mass spectrometry characterization of alpha-pinene ozonolysis SOA, Atmos. Environ., 46, 164–172, doi:10.1016/j.atmosenv.2011.10.003, 2012.

Seinfeld, J. and Pandis, S.: Atmospheric Chemistry and Physics: From Air Pollution to Climate Change, Wiley, Hoboken, 2006.

Shilling, J. E., Chen, Q., King, S. M., Rosenoern, T., Kroll, J. H., Worsnop, D. R., McKinney, K. A., and Martin, S. T.: Particle mass yield in secondary organic aerosol formed by the dark

ozonolysis of α-pinene, Atmos. Chem. Phys., 8, 2073–2088, doi:10.5194/acp-8-2073-2008, 2008.

Spracklen, D. V., Jimenez, J. L., Carslaw, K. S., Worsnop, D. R., Evans, M. J., Mann, G. W., Zhang, Q., Canagaratna, M. R., Allan, J., Coe, H., McFiggans, G., Rap, A., and Forster, P.: Aerosol mass spectrometer constraint on the global secondary organic aerosol budget, Atmos. Chem. Phys., 11, 12109–12136, doi:10.5194/acp-11-12109-2011, 2011.

Su, F., Calvert, J. G., and Shaw, J. H.: Mechanism of the photooxidation of gaseous formaldehyde, J. Phys. Chem., 83, 3185–3191, doi:10.1021/j100488a001, 1979.

Veres, P., Roberts, J. M., Warneke, C., Welsh-Bon, D., Zahniser, M., Herndon, S., Fall, R., and de Gouw, J.: Development of negative-ion proton-transfer chemical-ionization mass spectrometry (NI-PT-CIMS) for the measurement of gas-phase organic acids in the atmosphere, Int. J. Mass Spectrom., 274, 48–55, doi:10.1016/j.ijms.2008.04.032, 2008.

Veres, P., Roberts, J. M., Burling, I. R., Warneke, C., de Gouw, J., and Yokelson, R. J.: Measurements of gas-phase inorganic and organic acids from biomass fires by negative-ion proton-transfer chemical-ionization mass spectrometry, J. Geophys. Rese.-Atmos., 115, D23302, doi:10.1029/2010JD014033, 2010.

Veres, P. R., Roberts, J. M., Cochran, A. K., Gilman, J. B., Kuster, W. C., Holloway, J. S., Graus, M., Flynn, J., Lefer, B., Warneke, C., and de Gouw, J.: Evidence of rapid production of organic acids in an urban air mass, Geophys. Res. Lett., 38, L17807, doi:10.1029/2011GL048420, 2011.

Vogel, A. L., Äijälä, M., Brüggemann, M., Ehn, M., Junninen, H., Petäjä, T., Worsnop, D. R., Kulmala, M., Williams, J., and Hoffmann, T.: Online atmospheric pressure chemical ionization ion trap mass spectrometry (APCI-IT-MSn) for measuring organic acids in concentrated bulk aerosol – a laboratory and field study, Atmos. Meas. Tech., 6, 431–443, doi:10.5194/amt-6-431-2013, 2013.

Wine, P. H., Astalos, R. J., and Mauldin, R. L.: Kinetic and mechanistic study of the hydroxyl + formic acid reaction, J. Phys. Chem., 89, 2620–2624, doi:10.1021/j100258a037, 1985.

Yatavelli, R. L. N. and Thornton, J. A.: Particulate Organic Matter Detection Using a Micro-Orifice Volatilization Impactor Coupled to a Chemical Ionization Mass Spectrometer (MOVI-CIMS), Aerosol Sci. Technol., 44, 61–74, doi:10.1080/02786820903380233, 2010.

Yatavelli, R. L. N., Lopez-Hilfiker, F., Wargo, J. D., Kimmel, J. R., Cubison, M. J., Bertram, T. H., Jimenez, J. L., Gonin, M., Worsnop, D. R., and Thornton, J. A.: A Chemical Ionization High-Resolution Time-of-Flight Mass Spectrometer Coupled to a Micro Orifice Volatilization Impactor (MOVI-HRToF-CIMS) for Analysis of Gas and Particle-Phase Organic Species, Aerosol Sci. Technol., 46, 1313–1327, doi:10.1080/02786826.2012.712236, 2012.

Yatavelli, R. L. N., Stark, H., Thompson, S. L., Kimmel, J. R., Cubison, M. J., Day, D. A., Campuzano-Jost, P., Palm, B. B., Hodzic, A., Thornton, J. A., Jayne, J. T., Worsnop, D. R., and Jimenez, J. L.: Semicontinuous measurements of gas-particle partitioning of organic acids in a ponderosa pine forest using a MOVI-HRToF-CIMS, Atmos. Chem. Phys., 14, 1527–1546, doi:10.5194/acp-14-1527-2014, 2014.

Yu, J., Cocker, DavidR, I., Griffin, R., Flagan, R., and Seinfeld, J.: Gas-Phase Ozone Oxidation of Monoterpenes: Gaseous and Particulate Products, J.Atmos. Chem., 34, 207–258, doi:10.1023/A:1006254930583, 1999.

Zahardis, J., Geddes, S., and Petrucci, G. A.: Improved Understanding of Atmospheric Organic Aerosols via Innovations in Soft Ionization Aerosol Mass Spectrometry, Anal. Chem., 83, 2409–2415, doi:10.1021/ac102737k, 2011.

Zhang, Q., Jimenez, J. L., Canagaratna, M. R., Allan, J. D., Coe, H., Ulbrich, I., Alfarra, M. R., Takami, A., Middlebrook, A. M., Sun, Y. L., Dzepina, K., Dunlea, E., Docherty, K., DeCarlo, P. F., Salcedo, D., Onasch, T., Jayne, J. T., Miyoshi, T., Shimono, A., Hatakeyama, S., Takegawa, N., Kondo, Y., Schneider, J., Drewnick, F., Borrmann, S., Weimer, S., Demerjian, K., Williams, P., Bower, K., Bahreini, R., Cottrell, L., Griffin, R. J., Rautiainen, J., Sun, J. Y., Zhang, Y. M., and Worsnop, D. R.: Ubiquity and dominance of oxygenated species in organic aerosols in anthropogenically-influenced Northern Hemisphere midlatitudes, Geophys. Res. Lett., 34, L13801, doi:10.1029/2007GL029979, 2007.